AD NUMBER

AD804869

NEW LIMITATION CHANGE

TO

Approved for public release, distribution unlimited

FROM

Distribution authorized to U.S. Gov't. agencies only; Administrative/Operational Use; DEC 1966. Other requests shall be referred to Defense Atomic Support Agency, Washington, DC 20301.

AUTHORITY

DASA ltr, 26 Sep 1967

DASA-1892-I

Weapons Radiation Shielding Handbook

Chapter 5 / Methods for Calculating Effects of Ducts, Access Ways, and Holes in Shields

by Wade E. Selph and H. Clyde Claiborne

Handbook Editors

Lorraine S. Abbott, H. Clyde Claiborne, and Charles E. Clifford

DEFENSE ATOMIC SUPPORT AGENCY

Washington, D. C. 20301

DASA-1892-I

WEAPONS RADIATION SHIELDING HANDBOOK

Chapter 5. Methods for Calculating Effects of Ducts, Access Ways, and Holes in Shields

by

Wade E. Selph and H. Clyde Claiborne

Handbook Editors

Lorraine S. Abbott, H. Clyde Claiborne, and Charles E. Clifford

DEFENSE ATOMIC SUPPORT AGENCY

Washington, D. C. 20301

Preparing Agency

OAK RIDGE NATIONAL LABORATORY

Oak Ridge, Tennessee

Operated by UNION CARBIDE CORPORATION

for the U. S. ATOMIC ENERGY COMMISSION

DASA Order No. EO-806-65,

Task A2-11.033

Preface

At the request of the Defense Atomic Support Agency, Oak Ridge National Laboratory has undertaken the preparation of a handbook to aid engineers charged with the responsibility of designing shields to protect military equipment and personnel in the vicinity of a nuclear weapons burst. This document constitutes one chapter of the Handbook, with other chapters to be published as they are completed. These will include a chapter defining the radiation sources insofar as is possible and practicable (Chapter 2), a chapter outlining methods for calculating the attenuation of weapons radiation through various media (Chapter 3), and a chapter presenting radiation albedos (Chapter 4). These four chapters, together with an introductory first chapter, will eventually be bound as Volume I of the Handbook. Volume II will consist of two or more additional chapters presenting engineering design methods that are based on the more sophisticated techniques described in Volume I. The intent is that the shield designer will use Volume I as a textbook and ready reference and Volume II as a guide for handling most of the problems with which he will be confronted.

In order to prepare this Handbook, it has been necessary for Oak Ridge National Laboratory to obtain the assistance of several consultants and subcontractors. For this chapter on ducts, for example, Wade E. Selph of Radiation Research Associates, Inc., performed the initial literature search and prepared the draft with which the co-author and the editors worked. Other chapters will similarly represent a cooperative effort of ORNL and other organizations.

As is always the case for handbooks, the authors and editors are relying heavily on suggestions, reviews, and criticisms of others as an aid in the development of the various chapters. The list of individuals who have contributed in this manner has already grown very large, and it would be almost impossible to acknowledge each person here. We do, however, wish to express appreciation to Lt. Col. Charles D. Daniel and Lt. Col. William A. Alfonte, who as past and present DASA Shielding Project Officers have handled the administration of the contract and assisted in establishing the scope of the Handbook. We also wish to acknowledge the assistance of several persons at Oak Ridge National Laboratory who by virtue of having worked in the radiation shielding field for a number of years are able to serve as on-the-spot authorities to help resolve problem areas as they arise in the various chapters. Those who have acted in this capacity for the duct chapter are V. R. Cain, R. E. Maerker, and D. K. Trubey.

Finally, we wish to thank Mrs. Virginia M. Hamrick, who by carefully reading each draft of this chapter, including galley and page proofs, has both improved the rhetoric and helped eliminate some of the usual errors that always creep into formal publications.

December 1966

Contents

5.0. INTRODUCTION 1

5.1. METHODS FOR CALCULATING RADIATION TRANSMISSION THROUGH DUCTS 2

5.1.1. Analytic Methods for Line-of-Sight Radiation 2
Rectangular Ducts 4
Rectangular Slots 5
Cylindrical Ducts 6
Long Cylindrical Annulus 7

5.1.2. Ray Analysis Technique 8
General Description 8
Application to Cylindrical Ducts 9
Application to Partially Penetrating Cylindrical Ducts 11
Comparison with Experiment 13

5.1.3. Analog Monte Carlo Method 14
General Description 14
Comparison with Experiment 15

5.1.4. Albedo Methods 16
General Description 16
Simon-Clifford Technique for Cylindrical Ducts 20
LeDoux-Chilton Technique for Rectangular Ducts 21
Monte Carlo Methods for Rectangular Ducts 22
Comparison with Experiment 23

5.1.5. Empirical Correlation for Rectangular Ducts 35

5.2. METHODS FOR CALCULATING RADIATION TRANSMISSION THROUGH SHIELDS CONTAINING VOIDS 35

5.2.1. Ray Analysis Technique for Single Voids 35

5.2.2. Flux Perturbation Technique for Single Voids 38

5.2.3. Technique for Small Randomly Spaced Voids 39

APPENDIX 5A. MACHINE PROGRAMS 40

5A.1. Ray Analysis Programs 40

5A.2. Analog Monte Carlo Programs 41

REFERENCES 42

5.0. Introduction

Most of the shields that are designed to protect military equipment or personnel from weapons radiations will contain air-filled holes of some type. They may consist of access ways to accommodate ventilating ducts or other utility pipes, passageways to allow personnel to enter the structure, or distributed voids resulting from the use of nonhomogeneous material in the structure. Since radiation traverses air-filled regions essentially unimpeded, these irregularities in an otherwise adequate shield can represent a serious problem for the shield designer.

The most effective method for reducing the amount of radiation that travels through such openings is to design the ducts or passageways so that they do not penetrate straight through the shield, as, for example, ducts which contain one or more bends. Radiation traveling through ducts of this kind collides with some of the surrounding shield material and consequently is attenuated to some small fraction of the incident quantity. Even if during such collisions particles are scattered back into the duct, their angles of reflection and their energies following reflection will probably prevent them from traveling on in the forward direction. Thus, the introduction of a bend will eliminate a significant fraction of the radiation which has entered the mouth of the duct. This is especially true for gamma rays, since high-energy gamma rays scattered at large angles suffer a considerable reduction in energy.

When the radiation being considered is neutrons, the problem is more severe in that neutrons can undergo many scatterings without being absorbed or substantially degraded in energy, the number of scatterings depending, of course, on the composition of the shield and the initial energy of the neutron. Consequently neutrons have a much higher probability for "streaming" through shield penetrations than gamma rays do. The problem is further complicated by the fact that neutrons can introduce new sources of gamma rays: those emitted when neutrons are captured and those produced when neutrons suffer inelastic scattering. These neutron-induced gamma rays, like those from the original source, are, of course, also reduced in intensity by the introduction of bends.

From the above discussion it is apparent that in a practical shield pipes should follow irregular paths and passageways should be designed with one or more right-angle turns. Any removable plugs required in a shield should be of the stepped-plug type so that radiation streaming around the plug will strike shielding material before it penetrates very far into the structure. But even with all these precautions, the radiation transmitted through holes may easily constitute the major fraction of the dose penetrating a shield. Thus in order to avoid over-designing and thereby increasing the costs associated with constructing ducts and passageways, the shield designer must be able to predict the effect of various types of openings for a given set of conditions.

Many of the methods that have been developed for estimating the effect of openings in reactor shields[1-3] can also be used for weapons radiation shields. (Initial weapons radiation is analogous to radiation from an operating reactor, and fallout radiation is similar to that from a shut-down reactor.) Differences will exist in the geometries and energy distributions of reactor and weapons sources and, in general, in the geometrical relationship between the shield and the openings in the shield, but they can be accounted for. A weapons radiation shield, as is demonstrated by the examples given in this chapter, is usually considered to be a thick-walled structure which surrounds a central cavity and is penetrated by a duct that is circular or rectangular in cross section. The radiation source is incident on the outside of the structure and enters the structure both by penetrating shielding material and by following the path of the duct.

For simple ducts (straight ducts) the component that will probably contribute most to the dose penetrating the structure will be the "line-of-sight" component which travels uninhibited from the mouth of the duct to the central cavity. Analytic methods for calculating this component are presented in Section 5.1.1. Another component which can be important for simple ducts is the radiation that reaches the duct through the surrounding shielding material, either as uncollided radiation that entered the shield in the direction of the duct or as

radiation that is scattered by the shielding material into the duct. These components are generally handled by the ray analysis technique discussed in Section 5.1.2.

More sophisticated techniques are required for treating more complicated duct geometries or for obtaining higher accuracy for the simple geometries. This means that the shield designer will have to resort to a computer program to perform calculations that involve a great many particle scatterings with consequent changes in direction and energy degradation. A number of analog Monte Carlo computer programs are available for such calculations, but, as is pointed out in Section 5.1.3, the amount of computer time required to use them is usually prohibitive. As a result, modified Monte Carlo programs have been developed for neutron transmission calculations which do not attempt to follow particle paths through the shielding material surrounding the duct but instead employ albedo theory to estimate reflectance from the duct walls. These programs are discussed in Section 5.1.4, along with other albedo techniques that have been devised for estimating gamma-ray transmission.

Finally, this chapter presents a few techniques for calculating the effects of holes or depressions in shields. Both single large voids and smaller voids distributed throughout the shield are considered. The techniques have been applied almost exclusively to gamma rays, but they are equally applicable to neutrons.

The applicability of most of the methods presented here is demonstrated by comparisons of calculated and experimental results. In a few cases additional experimental data are included to provide empirical results which will be of value for future reference.

5.1. Methods for Calculating Radiation Transmission Through Ducts

5.1.1. ANALYTIC METHODS FOR LINE-OF-SIGHT RADIATION

For the case of a duct that penetrates straight through a thick shield and has dimensions that are large compared with the mean free path of the penetrating radiations, the "line-of-sight" radiation, that is, the radiation which travels directly from the source to the detector through the duct, can be the most significant portion of the total radiation reaching the detector. A simple example of this situation is that of a disk source and an adjacent shield which has a cylindrical duct passing completely through it. For a detector located on the duct axis three or more source diameters from the source, the ratio of the line-of-sight radiation through the duct to the uncollided radiation reaching the detector through the shield is approximately the ratio of the cross-sectional area of the duct divided by the area of the disk source times the attenuation of the shield. Thus if the area of the source is ten times the area of the duct and the shield is approximately three mean free paths thick, the line-of-sight component is two-thirds of the total uncollided radiation reaching the detector.

In more complex situations, for example, in the case of a weapon burst and the subsequent scattering of the radiation before it enters the duct, the source can be treated as a plane source at a given location and will have a particular angular distribution dependent upon the geometry of the actual source and its surrounding medium. If it is assumed that the source is a plane source at the duct opening and that the ratio of the duct length to diameter is large, all line-of-sight points are approximately equidistant from the other end of the duct and may be treated collectively as an

equivalent point source. If the plane source is treated as having isotropic current, the equivalent point intensity is the product SN_0, where N_0 is the particle emission rate per unit area and time and S is the area on the source plane that is viewed through the duct from the point of interest. For nonisotropic emitters each differential area element must be weighted by the angular distribution in performing the integral over the source area. For complex source distributions and geometries, the integral over the source must be evaluated numerically. However, for many geometries and source angular distributions which may be expressed analytically, it is possible to derive formulas for the line-of-sight flux or current through an opening.

The sections below present several methods that have been developed for computing the line-of-sight flux in simple ducts of various geometries. For these cases the source is assumed to be a plane which is normal to the axis of the duct and covers the duct entrance. Two types of source angular distributions are considered: an isotropic distribution and cosine distributions. Here isotropic distribution refers to radiation that is assumed to be given off in all directions in the forward hemisphere with equal probability but with no emission in the backward hemisphere. Thus if a surface emission is N_0 particles/cm^2 sec, then the number of particles emitted into any unit solid angle is $N_0/2\pi$ particles/cm^2 steradian sec.

For cosine distributions the radiation leakage through a unit area on the surface of a self-absorbing volume-distributed source is most intense in the direction normal to the surface, and the variation with the angle θ from the normal is approximated by a cosine function, in which case the number of particles emitted per unit solid angle is $N_0 \cos\theta/\pi$ particles/cm^2 steradian sec.

Other functions have been used to describe sources which have more forwardly peaked angular distributions than that given by $\cos\theta$. In general, most of these can be represented by $\cos^n\theta$, where n may be as large as 20. The $\cos^n\theta$ function has been useful in representing a leakage current or a flux at a shield surface from an absorbing source region in which the activity per unit volume increases with depth.

Two types of plane sources have been used in analytical expressions derived for the transmission of uncollided particles through ducts. In one type the source strength is defined by a particle *emission rate*, which in this chapter will always be designated as N_0 (particles/cm^2 sec). In the other type, the source strength is defined by a *flux*, which will be designated here as Φ_0 (particles/cm^2 sec). This second source is the more natural one for use in shield design. It is used almost exclusively for shelter design since an analysis of the transmission of radiation from a weapon burst through ambient atmosphere will yield a flux which will then be used as the source at the duct entrance. (An example of an isotropic plane source described by a particle emission rate is a converter plate such as the one that was used in the Lid Tank Shielding Facility at Oak Ridge National Laboratory as a source for shielding experiments.)

In calculating the flux in a duct, care must be taken to ensure that the proper source angular distribution is used in a given situation since there is a basic difference in the two sources. This is because a particle emission rate is a current and therefore is referenced to a square centimeter of the source area, whereas a flux is always referenced to a square centimeter of area that is normal to the particle direction. Therefore, to correct for the different orientation of the flux-source reference area, it is necessary to multiply the flux passing through that area by $\cos\theta$ in order to project the reference area back to the source plane. That is, the relationship between the angular current $J(\cos\theta)$ from the first type of source and the angular flux $\Phi(\cos\theta)$ from the second type of source is

$$J(\cos\theta) = \cos\theta\,\Phi(\cos\theta)\,. \qquad (5.1)$$

The effect of the difference in the two sources can be shown by the following example. The uncollided flux in a duct is to be calculated for a given angular distribution $g(\cos\theta)$ (particles/cm^2 steradian sec) specified on the source plane. If $g(\cos\theta)$ is the normalized angular *current* [the normalization condition on $g(\cos\theta)$ is $\int_0^1 g(\cos\theta)\,2\pi\,d(\cos\theta) = 1$], then the flux at any point in the duct is

$$\int_S N_0\, g(\cos\theta)\,\frac{dS}{r^2}\,. \qquad (5.2)$$

where N_0 is the total emission rate, dS is a differential area on the source plane S, and r is the distance between dS and the detector. If, on the other hand, $g(\cos\theta)$ is the normalized angular *flux*, then the flux in the duct is

$$\int_S \Phi_0 g(\cos\theta) \frac{\cos\theta}{r^2} dS , \qquad (5.3)$$

where Φ_0 is the total or scalar flux at the source plane.

A general relation between the emission rate and the flux may be derived for the very useful case of the $\cos^n\theta$ distribution by defining the angular emission rate (angular current) as

$$J(\cos\theta) = \frac{n+1}{2\pi} N_0 \cos^n\theta . \qquad (5.4)$$

That Eq. 5.4 is properly normalized is seen by calculating the total emission rate:

$$\int_0^1 \frac{n+1}{2\pi} N_0 \cos^n\theta \, 2\pi \, d(\cos\theta) = N_0 . \qquad (5.5)$$

The corresponding expression for the total flux, Φ_0, at the source plane is then

$$\Phi_0 = \int_0^1 \frac{n+1}{2\pi} N_0 \frac{\cos^n\theta}{\cos\theta} 2\pi \, d(\cos\theta)$$

$$= \frac{n+1}{n} N_0 . \qquad (5.6)$$

It is evident that Eq. 5.6 does not hold when $n = 0$; in fact, the flux is not defined on the source plane when the emission rate is isotropic.

For all the different duct geometries included in the following discussion, the flux Φ or leakage current J at the exit plane of the duct is expressed in the same units as the source strength, e.g., particles/cm^2 sec. In order to obtain the total leakage flux or current through the exit plane of the duct, it is necessary to integrate Φ or J over the exit area.

Rectangular Ducts. – The work of Hubbell *et al.*[4] on radiation from uniform rectangular sources with arbitrary angular distributions is directly applicable to the calculation of the uncollided flux along the axis of a rectangular duct. In that work, radiation crossing a plane S (cross-sectional area of duct normal to axis) is assumed to be known and is designated by an arbitrary function $g(\cos\theta)$, which is the angular flux and represents the number of particles traveling in the direction θ with respect to the duct axis per unit solid angle, unit time, and unit area normal to direction θ (neutrons/cm^2 sec steradian). The flux at any point along the axis is expressed by

$$\Phi = \int_S g(\cos\theta) \, d\Omega_s(\theta) , \qquad (5.7)$$

where $d\Omega_s(\theta)$ is the differential solid angle subtended from an isotropic detector by the surface dS (see Fig. 5.1) and is equal to

$$\frac{\cos\theta \, dS}{r^2} .$$

A solution to Eq. 5.7 was developed by Hubbell *et al.* in terms of completely separable source and geometry functions and was expressed as

$$\Phi = \sum_{l=0}^{\infty} \frac{2l+1}{2} g_l p_l(a,b) , \qquad (5.8)$$

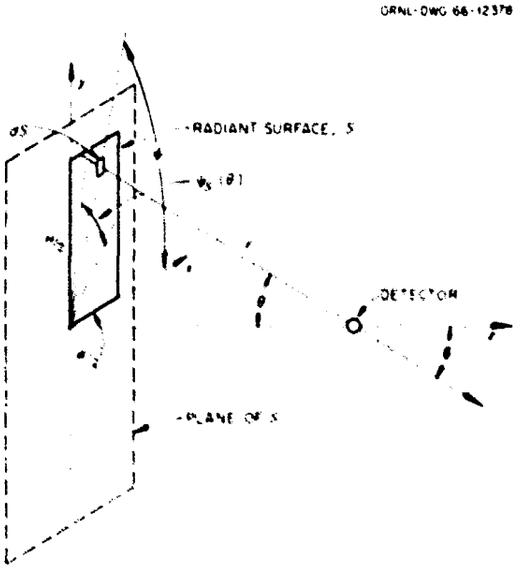

Fig. 5.1. Schematic of Source Plane and Detector Position for a Rectangular Duct.

where a is the ratio of the half height ($H/2$) to the length (Z) of the duct, b is the ratio of the half width ($W/2$) to the length, and g_l and p_l are coefficients of Legendre polynomial expansions of the source and geometry functions respectively. With these definitions of a and b, Eq. 5.8 gives the flux at a corner for the quarter plane limned in Fig. 5.1. The flux at the center line for the full plane is obtained by multiplying Eq. 5.8 by 4.

The coefficients are calculated by

$$g_l = \int_{-1}^{+1} g(\cos\theta)\, P_l(\cos\theta)\, d(\cos\theta) \quad (5.9)$$

and

$$p_l(a,b) = \int_S P_l(\cos\theta)\, d\Omega_s(\theta)\,, \quad (5.10)$$

where the $P_l(\cos\theta)$'s are the Legendre polynomials.

Although the solution of Eq. 5.10 is in terms of a finite series, the terms become progressively more complicated with increasing l and only the first four p_l's were evaluated analytically. Using an electronic computer, Hubbell *et al*. numerically evaluated p_l's for $0 \leq l \leq 13$ over a grid of a and b values of $0.1 \leq b \leq a \leq 20$. Using these tabulated values and the g_l's determined for any arbitrary $g(\cos\theta)$, the flux along the axis or at the corner of a duct can be calculated with Eq. 5.8.

For the special and useful case of the $\cos^n\theta$ distribution,

$$g(\cos\theta) = \frac{(n+1)\,\Phi_0}{2\pi}\cos^n\theta\,, \quad (5.11)$$

where Φ_0 is the source strength that is represented by a scalar flux obtained by integrating the angular flux over all angles in the direction of the duct entrance. Consequently, Eq. 5.11 is properly normalized since

$$\int_0^1 \frac{n+1}{2\pi}\cos^n\theta\, 2\pi\, d(\cos\theta) = 1\,. \quad (5.12)$$

For integral values of n, Eq. 5.11 can be expanded into a finite number of Legendre polynomials, and, in principle, an analytical solution to Eq. 5.8 can be obtained. However, the solution rapidly becomes unwieldly for progressively higher values of n. The fluxes along the axis of a rectangular duct for the isotropic flux source ($n = 0$) and for more forwardly peaked sources ($n = 1$ and 2) when uniform over the duct mouth are given below. The flux at a corner of a rectangle with dimensions $W/2 \times H/2$ is one-fourth of that calculated by Eqs. 5.13 through 5.15.

For $n = 0$:

$$\Phi = \frac{2\Phi_0}{\pi}\tan^{-1}\frac{ab}{\sqrt{1+a^2+b^2}}\,. \quad (5.13)$$

For $n = 1$:

$$\Phi = \frac{2\Phi_0}{\pi}\left[\frac{a}{\sqrt{1+a^2}}\tan^{-1}\frac{b}{\sqrt{1+a^2}} + \frac{b}{\sqrt{1+b^2}}\tan^{-1}\frac{a}{\sqrt{1+b^2}}\right]. \quad (5.14)$$

For $n = 2$:

$$\Phi = \frac{3\Phi_0}{\pi}\left[\frac{ab}{\sqrt{1+a^2+b^2}}\left(\frac{1}{1+a^2}+\frac{1}{1+b^2}\right)\right]. \quad (5.15)$$

As the distance between the source and detector becomes large with respect to cross-section dimensions, the inverse tangent in Eq. 5.13 approaches ab and the terms in the brackets in Eqs. 5.14 and 5.15 approach $2ab$ or $WH/2Z^2$. In general, it can be shown that for long thin ducts of rectangular cross section

$$\Phi = \frac{(n+1)\,WH\Phi_0}{2\pi Z^2}\,. \quad (5.16)$$

Equation 5.16 represents a lower limit for a point source (emitting only into the forward hemisphere) and also for a plane source (for a detector far away from the duct entrance) since the flux scattered from the wall of the duct is not included. In many practical cases the contribution to the dose by the scattered flux will be of the same order as or smaller than the contribution by the uncollided flux. (The dose is calculated by summing the product of the flux and the appropriate dose response function for each energy group of neutrons.)

Rectangular Slots. – The geometry used in the derivations of the approximate equations for a rectangular slot is shown in Fig. 5.2. The dimensions of the duct adjacent to the source plane are W by H and the distance from the source plane to

ORNL-DWG 66-10406

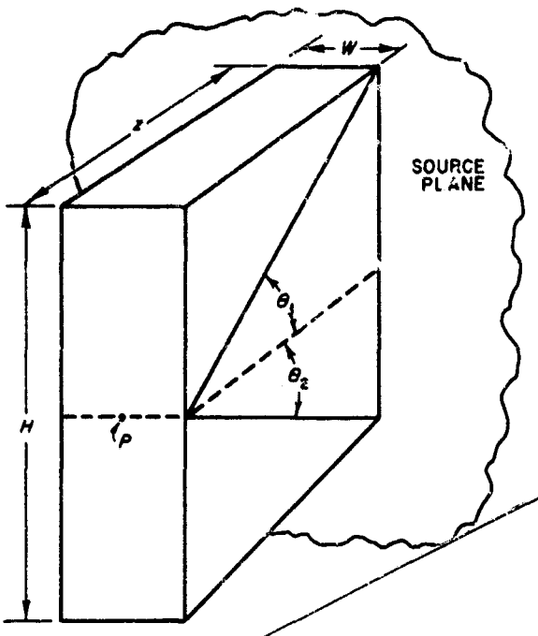

Fig. 5.2. Rectangular Slot Geometry. Source plane and exit plane are normal to Z direction.

the exit end of the slot is Z. When $H \gg W$ (say, $H/W > 5$), the exposed source can be approximated by a line source, and the line-of-sight flux Φ and the leakage current J at any point P along the horizontal axis on the exit end of the slot by

$$\Phi_i = \frac{N_0 W}{2\pi Z}(\theta_1 + \theta_2), \qquad (5.17)$$

$$J_i = \frac{N_0 W}{2\pi Z}(\sin\theta_1 + \sin\theta_2); \qquad (5.18)$$

$$\Phi_c = \frac{N_0 W}{\pi Z}(\sin\theta_1 + \sin\theta_2), \qquad (5.19)$$

$$J_c = \frac{N_0 W}{4\pi Z}[\sin 2\theta_1 + \sin 2\theta_2 + 2(\theta_1 + \theta_2)]; \qquad (5.20)$$

where N_0 is the source emission rate per unit area or current, θ is expressed in radians, and the subscripts i and c refer to isotropic and cosine sources respectively.

If the slot dimensions are such that $Z \gg H$ and $\theta_1 + \theta_2 \to \pi$, the above equations become

$$\Phi_i = \frac{N_0 W}{2Z}, \qquad (5.21)$$

$$J_i = \frac{N_0 W}{\pi Z}; \qquad (5.22)$$

$$\Phi_c = \frac{2N_0 W}{\pi Z}, \qquad (5.23)$$

$$J_c = \frac{N_0 W}{2Z}. \qquad (5.24)$$

The rectangular slot can be considered a special case of the rectangular duct for the condition when $W \to 0$, and Eq. 5.19 can be derived by taking the limit of Eq. 5.13 as $W \to 0$. In the limiting process an apparent anomaly occurs; the answer is in terms of Φ_0, the flux at the source. However, the fluxes on a line source for both isotropic and cosine distributions are always infinite. Consequently, in taking the limit of Eq. 5.13 as $W \to 0$, Φ_0 should be converted to an emission rate ($2N_0$).

Cylindrical Ducts. – Consider a cylindrical duct of radius a normal and adjacent to a plane source with the detector a distance Z from the source plane and on the duct axis (Fig. 5.3). For an isotropic current or emission rate on the source plane,

ORNL-DWG 66-10409

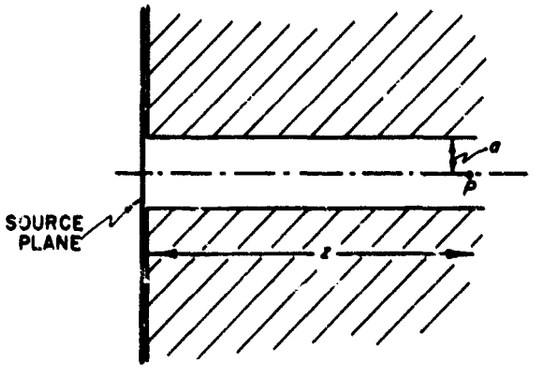

Fig. 5.3. Geometry for Cylindrical Duct Adjacent to Plane Source.

the line-of-sight flux at any point P is given by

$$\Phi_i = \frac{N_0}{2} \ln [1 + (a/Z)^2] , \qquad (5.25)$$

and the current parallel to the axis of the cylinder is given by

$$J_i = N_0 \left[1 - \frac{1}{\sqrt{1 + (a/Z)^2}} \right] . \qquad (5.26)$$

For a cosine current source

$$\Phi_c = 2N_0 \left[1 - \frac{1}{\sqrt{1 + (a/Z)^2}} \right] \qquad (5.27)$$

and

$$J_c = \frac{N_0 a^2}{Z^2[1 + (a/Z)^2]} . \qquad (5.28)$$

Equations 5.27 and 5.28 can be expressed in terms of an isotropic flux at the source plane by letting $2N_0 = \Phi_0$.

For $Z >> a$, say, $Z/a > 5$, it can be shown that these equations approach

$$\Phi_i \cong J_i \cong \frac{N_0(\pi a^2)}{2\pi Z^2} \cong \frac{N_0 a^2}{2Z^2} , \qquad (5.29)$$

which is the same result for a point source of strength $N_0(\pi a^2)$, and

$$\Phi_c \cong J_c \cong \frac{N_0(\pi a^2)}{\pi Z^2} \cong \frac{N_0 a^2}{Z^2} . \qquad (5.30)$$

If the condition of a long duct of small cross-sectional area is met, Eqs. 5.29 and 5.30 will also hold for a straight duct of any cross-sectional geometry if πa^2 is replaced by the cross-sectional area of the duct.

Long Cylindrical Annulus. – The geometry for a long cylindrical annular duct is shown in Fig. 5.4. The duct is bounded by two cylindrical surfaces having radii a_1 and a_2. For the conditions $Z >> a_2 - a_1$ and $a_2 >> a_2 - a_1$ and an isotropic source N_0, the average line-of-sight flux $\bar{\Phi}$ along the duct

ORNL-DWG 66-10418

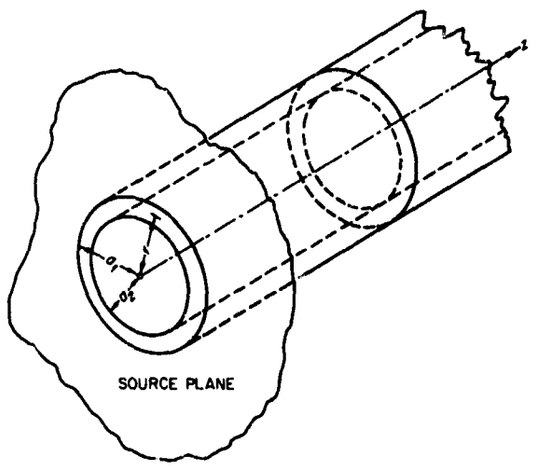

Fig. 5.4. Geometry for Cylindrical Annulus Adjacent to Plane Source.

axis may be approximated by

$$\bar{\Phi} = \frac{MN_0}{2\pi Z^2} [(2a_2^2 - a_1^2) \cos^{-1} (a_1/a_2) - a_1 \sqrt{a_2^2 - a_1^2}] . \qquad (5.31)$$

The average leakage current $\bar{J}$ for the isotropic source N_0 can also be obtained from Eq. 5.31 by setting $M = 1$. The equation[3] for the flux at any radius r ($a_1 \leq r \leq a_2$) within the annulus is

$$\Phi(r,Z) = \frac{MN_0 a_2^2}{\pi Z^2} [1 - (a_1/a_2)^2 \cos^{-1} (a_1/r) + \cos^{-1} (a_1/a_2) - (a_1/a_2) [1 - (a_1/a_2)^2]^{1/2}] , \qquad (5.32)$$

where $M = 1$ for an isotropic source and $M = 2$ for a cosine source, and r and Z are the cylindrical coordinates of the point P at which the flux is given. Equation 5.32 is equivalent to

$$\Phi(r,Z) = \frac{MN_0 S}{2\pi Z^2} , \qquad (5.33)$$

where S is the area on the source plane that is viewed from the point $P(r,Z)$.

5.1.2. RAY ANALYSIS TECHNIQUE

General Description. – In addition to the line-of-sight radiation, the flux reaching a detector located near the exit end of a simple duct includes radiation that enters the duct through its walls.* This contribution consists of two components: radiation that travels directly from the source to the detector through shielding material without an interaction (uncollided flux) and radiation that scatters in the direction of the detector as a result of interactions with the shield. A method useful in calculating these components is the ray analysis method, which has frequently been applied to shield attenuation calculations.

The basic assumption of the ray analysis technique, also referred to as the point kernel method, is that the radiation transmission is a function only of the path lengths through each material or void encountered along a straight line between the source point and the detector. This assumption is entirely correct for predicting the uncollided flux, and for geometries in which the scattered flux becomes important, the collided fluxes can be accounted for to a first approximation by using buildup factors for gamma rays and removal cross sections for neutrons. Although the accuracy of the method is highly dependent on the particular configuration being considered, it can be applied to simple ducts with considerable confidence since the radiation reaching the detector largely consists of the uncollided component.

To illustrate the method, consider, for example, the case of a point detector P removed a distance r from a point source at Q, where the straight-line path between the two points passes through both shielding material and void (see Fig. 5.5). The flux at the detector is given by

$$\Phi_p = \frac{N_p}{4\pi r^2} K , \qquad (5.34)$$

where N_p is the point-source strength and K is the material attenuation kernel for all the materials located between the source and the dose point.

ORNL DWG 66-10402

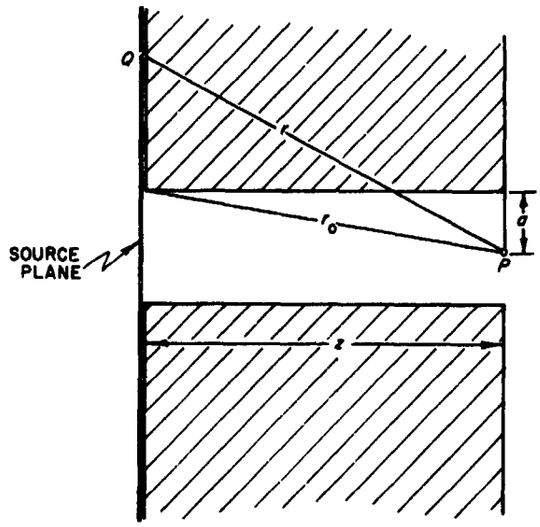

Fig. 5.5. Geometry for Ray Analysis Calculation of Radiation Component Arriving Through Wall of Duct.

If only the uncollided flux at P is considered,

$$K = \exp\left(-\sum_i t_i \frac{1}{l_i}\right) , \qquad (5.35)$$

where l_i is the mean free path of a particle and t_i is the straight-line path through the ith material. When the radiation being considered consists of neutrons, $1/l_i$ is usually expressed in terms of the total macroscopic cross section Σ_{T_i} (cm^{-1}) and t_i is given in centimeters. When gamma rays are being treated, $1/l_i$ is expressed as the mass absorption coefficient μ_i/ρ_i (cm^2/g) and t_i is in units of cm^2/g. If the thickness t_i is expressed in centimeters, then $1/l$ is replaced by the linear attenuation coefficient (cm^{-1}), which is the total macroscopic cross section for gamma rays.

Equation 5.35 can be modified to include a first-order approximation of the scattered gamma radiation by multiplying the right-hand side by a buildup factor:

$$K = B(t_1, t_2, \ldots) \exp\left(-\sum_i t_i \frac{1}{l_i}\right) . \qquad (5.36)$$

The equation can be modified similarly to include a first-order approximation of scattered neutrons

*Radiation that enters the mouth of the duct in a direction other than the direction of the detector but subsequently scatters in the duct wall toward the detector also contributes to the flux. For simple ducts the contribution from this source is usually small, but for ducts with bends it becomes the dominant component as is discussed in Sections 5.1.3 and 5.1.4.

by substituting the neutron removal cross section* Σ_R for Σ_T:

$$K = \exp - \sum \Sigma_{R_i} t_i \ . \qquad (5.37)$$

In the above discussion the assumption is made that the flux at the point P is the same as it would be if all the particles traveling from Q to P, including those that are scattered, encounter effectively the same amount of attenuating material that exists along the line from Q to P. If significantly less material is encountered by some particles, the total flux at P determined by Eq. 5.34 may be underestimated. Conversely, if significantly more material is encountered, the flux may be overestimated. Also, Eq. 5.34 neglects the effects of material-void interfaces or interfaces between dissimilar materials encountered along the ray and in the surrounding regions.

In the use of the ray analysis method to integrate over a source plane or source volume, the possible inaccuracy involved in the contribution of an individual source point may be masked by the contributions from other points. There are, of course, complex geometries and material combinations for which the simple ray analysis techniques do not predict the radiation fluxes with any satisfactory degree of accuracy. However, ray analysis is in many cases quite adequate and is an easily applied method.

There are also cases in which the accuracy requirements and the complexity of the problem geometry may prohibit the use of the approximations given in this section except as first estimates. In such situations numerical integration may be used to obtain a ray analysis solution either by hand or by machine calculations. The decision to use a computer will, in general, be based on the number of calculations that must be performed to give the desired degree of accuracy. Several computer programs have been developed which facilitate point-kernel integrations. Some of their common features, as well as brief descriptions of a few specific programs that are available, are given in the appendix to this chapter.

Application to Cylindrical Ducts. – For the case in which the duct shown in Fig. 5.5 is a cylindrical duct of radius a penetrating an infinite slab shield adjacent to an infinite plane isotropic source, the uncollided flux at P that arrives through the duct walls is

$$\Phi_i = N_0 \int_{r_0}^{\infty} e^{-\mu l(r)} \frac{dr}{r}, \qquad (5.38)$$

where

N_0 = surface emission rate or current,

$l(r)$ = path length in the shield which lies along r

$$= r\left(1 - \frac{a}{\sqrt{r^2 - Z^2}}\right),$$

μ = linear attenuation coefficient.

The corresponding flux for a cosine source is given by

$$\Phi_c = 2N_0 \int_{r_0}^{\infty} e^{-\mu l(r)} \frac{Z}{r^2} dr \ . \qquad (5.39)$$

Equations 5.38 and 5.39 are not amenable to straightforward analytical solutions, although values of the integrals may be found in tables of mathematical functions. Certain approximations, based on a Taylor expansion of $l(r)$, have been given by Chase,[1] but they are valid only for large values of a/Z. Trubey[5] evaluated the equations numerically for a unit surface source intensity (for $N_0 = 1$). The results are shown in Tables 5.1 and 5.2 as a function of the ratio of the duct radius to the length (a/Z) and the shield thickness μZ, where μZ is measured in relaxation lengths (or mean free paths determined from material cross sections).

The data for the uncollided flux given in Tables 5.1 and 5.2 may be used to estimate the total radiation arriving through the duct wall, provided that the parameters a/Z and μZ are measured in terms of an effective relaxation length, $\lambda = 1/\mu$, which accounts for the radiation scattered in the direction of P by the shield. Relaxation length values which include scattering may be obtained from experimental data or from basic calculations of penetration through the material by Monte Carlo or moments methods. When such data are used they should be for the same material and the same energy (or spectrum) as those being considered in the duct penetration problem. Neutron removal cross sections or gamma-ray buildup factors, both

*Removal cross sections are valid only for those cases in which the shielding materials are followed by a thick layer of water or, to a lesser extent, for those cases in which mixtures containing hydrogenous materials are used (see Chapter 3).

Table 5.1. Uncollided Flux at Exit of Cylindrical Duct Due to Radiation Arriving Through Duct Walls (Isotropic Source)[a]

$\left(\frac{a}{Z}\right)$	Flux Per Unit Surface Source Intensity for Shield Thickness of					
	$\mu Z = 0.1$[b]	$\mu Z = 0.2$	$\mu Z = 0.5$	$\mu Z = 1.0$	$\mu Z = 2.0$	$\mu Z = 5.0$
0.001	1.823	1.223	0.5602	0.2198	0.04912	1.166×10^{-3}
0.002	1.823	1.223	0.5607	0.2207	0.04935	1.184×10^{-3}
0.005	1.824	1.224	0.5620	0.2215	0.05002	1.242×10^{-3}
0.01	1.825	1.226	0.5643	0.2235	0.05119	1.349×10^{-3}
0.02	1.828	1.229	0.5688	0.2278	0.05363	1.614×10^{-3}
0.05	1.834	1.239	0.5820	0.2406	0.06171	2.977×10^{-3}
0.1	1.842	1.254	0.6024	0.2613	0.07621	7.042×10^{-3}
0.2	1.851	1.272	0.6360	0.2982	0.1049	1.795×10^{-2}
0.5	1.825	1.277	0.6841	0.3659	0.1687	5.223×10^{-2}
0.75	1.765	1.240	0.6804	0.3819	0.1923	6.990×10^{-2}
1.0	1.689	1.185	0.6560	0.3767	0.1980	7.753×10^{-2}

[a]From D. K. Trubey, *A Calculation of Radiation Penetration of Cylindrical Duct Walls*, ORNL-CF-63-2-64 (Feb. 28, 1963).

[b]Number of relaxation lengths.

Table 5.2. Uncollided Flux at Exit of Cylindrical Duct Due to Radiation Arriving Through Duct Walls (Cosine Source)[a]

$\left(\frac{a}{Z}\right)$	Flux Per Unit Surface Source Intensity for Shield Thickness of					
	$\mu Z = 0.1$[b]	$\mu Z = 0.2$	$\mu Z = 0.5$	$\mu Z = 1.0$	$\mu Z = 2.0$	$\mu Z = 5.0$
0.001	1.445	1.149	0.6539	0.2976	0.07544	0.002026
0.002	1.446	1.149	0.6545	0.2983	0.07582	0.002059
0.005	1.446	1.150	0.6564	0.3002	0.07698	0.002166
0.01	1.447	1.152	0.6595	0.3034	0.07896	0.002365
0.02	1.450	1.156	0.6657	0.3100	0.08314	0.002862
0.05	1.455	1.166	0.6836	0.3298	0.09703	0.005458
0.1	1.459	1.179	0.7095	0.3610	0.1217	0.01323
0.2	1.453	1.188	0.7462	0.4120	0.1682	0.03343
0.5	1.339	1.116	0.7510	0.4714	0.2494	0.08728
0.75	1.190	0.9949	0.6827	0.4465	0.2553	0.1036
1.0	1.036	0.8643	0.5953	0.3956	0.2340	0.1014

[a]From D. K. Trubey, *A Calculation of Radiation Penetration of Cylindrical Duct Walls*, ORNL-CF-63-2-64 (Feb. 28, 1963).

[b]Number of relaxation lengths.

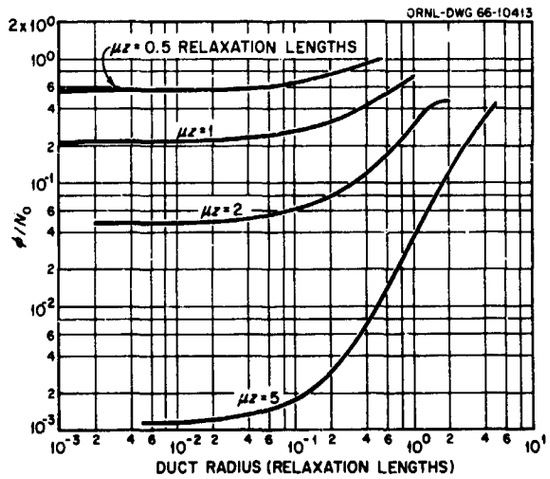

Fig. 5.6. Effect of Duct Radius and Shield Thickness on Total Uncollided Flux Reaching Exit of Cylindrical Duct (Isotropic Source).

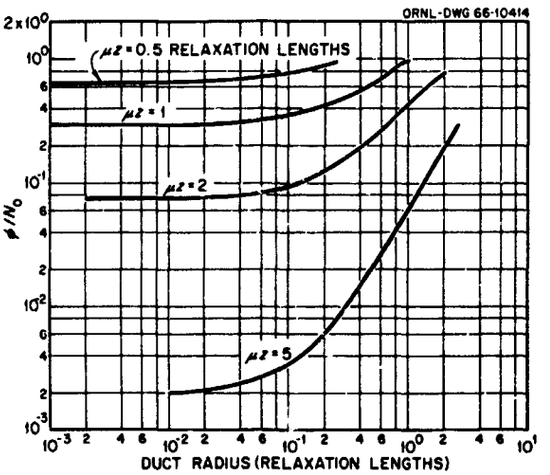

Fig. 5.7. Effect of Duct Radius and Shield Thickness on Total Uncollided Flux Reaching Exit of Cylindrical Duct (Cosine Source).

of which are derived from basic penetration data, may be used in obtaining values of λ. In this use of the data, the assumption is made that the total attenuation is exponential; that is, the relaxation length does not vary with penetration depth.

Figures 5.6 and 5.7, which are based on Trubey's data,[5] show the variation with shield thickness and duct size of the total flux, including the line-of-sight component, reaching the center of the duct exit. All parameters are measured in terms of the shield material relaxation length. The flux is given for an infinite plane source of unit source strength (e.g., 1 particle/cm^2 sec).

The relative importance of the line-of-sight radiation discussed in Section 5.1.1 and of the uncollided radiation that leaks through a duct wall is illustrated by some additional calculations by Trubey given in Table 5.3. Here it is apparent that the ratio of the line-of-sight component to the total uncollided flux depends strongly on the ratio of the duct radius to the length (a/Z) and on the shield thickness μZ. These ratios represent an upper limit since the buildup of the flux due to scattering has not been considered. The ratios are applicable to either fast neutrons or gamma rays provided the shield thickness is defined in terms of the number of relaxation lengths. An examination of the data in Table 5.3 reveals that the radiation which penetrates the wall of a duct dominates over that from the source in the mouth of the duct for small-diameter ducts that penetrate thin shields. As the duct diameter increases and/or the shield thickness increases, the line-of-sight component becomes of greater importance.

If the duct is filled with a lightly attenuating medium, formulas similar to those in preceding sections could be derived which include exponential attenuation through the duct material in the kernel integration. This condition would tend to decrease further the importance of the source at the mouth of the duct.

Application to Partially Penetrating Cylindrical Ducts. – The radiation transmitted through the walls of a cylindrical duct that penetrates only part of the shield and is not adjacent to the source may be calculated by the ray analysis technique in much the same manner as for a completely penetrating duct. Consider, for example, the duct shown in Fig. 5.8*a*. Equations 5.38 and 5.39 may be applied to this geometry merely by changing the lower limit of integration from r_0 to Z. As before, $l(r)$ is that portion of r which lies inside the shield.

An alternative to numerical integration of these equations for each case would be to determine the flux penetrating an infinite slab of thickness t (see Section 5.2.1), use this as a source strength input to the ducted shield of thickness $Z - t$, and evaluate using the data presented in the previous section (Figs. 5.6 and 5.7). In the absence of more definitive data, a more forwardly peaked distribution

Table 5.3. Ratio of Line-of-Sight Radiation to Total Uncollided Flux in Duct[a]

$\left(\frac{a}{Z}\right)$	Fraction of Total Flux for Shield Thickness of					
	$\mu Z = 0.1$[b]	$\mu Z = 0.2$	$\mu Z = 0.5$	$\mu Z = 1.0$	$\mu Z = 2.0$	$\mu Z = 5.0$
	Isotropic Infinite-Plane Source					
0.001	$<10^{-6}$	$<10^{-6}$	$<10^{-6}$	$<10^{-5}$	$<10^{-4}$	$<10^{-3}$
0.002	$<10^{-5}$	$<10^{-5}$	$<10^{-5}$	$<10^{-5}$	$<10^{-4}$	0.002
0.005	$<10^{-5}$	$<10^{-4}$	$<10^{-4}$	$<10^{-4}$	$<10^{-3}$	0.010
0.01	$<10^{-4}$	$<10^{-4}$	$<10^{-4}$	10^{-3}	0.001	0.038
0.02	$<10^{-3}$	$<10^{-3}$	10^{-3}	10^{-3}	0.004	0.11
0.05	$<10^{-3}$	0.001	0.002	0.005	0.020	0.29
0.1	0.003	0.004	0.008	0.019	0.062	0.42
0.2	0.011	0.015	0.031	0.062	0.16	0.52
0.5	0.059	0.083	0.14	0.23	0.40	0.68
0.75	0.11	0.15	0.25	0.37	0.53	0.76
1.0	0.17	0.23	0.34	0.48	0.64	0.82
	Cosine Infinite-Plane Source					
0.001	$<10^{-6}$	$<10^{-6}$	$<10^{-5}$	$<10^{-5}$	$<10^{-4}$	$<10^{-3}$
0.002	$<10^{-5}$	$<10^{-5}$	$<10^{-5}$	$<10^{-4}$	$<10^{-4}$	0.002
0.005	$<10^{-4}$	$<10^{-4}$	$<10^{-4}$	$<10^{-4}$	$<10^{-3}$	0.011
0.01	$<10^{-4}$	$<10^{-4}$	$<10^{-3}$	$<10^{-3}$	0.001	0.040
0.02	$<10^{-3}$	$<10^{-3}$	$<10^{-3}$	0.002	0.005	0.12
0.05	0.002	0.002	0.004	0.008	0.025	0.27
0.1	0.007	0.008	0.014	0.027	0.076	0.43
0.2	0.026	0.031	0.050	0.12	0.19	0.54
0.5	0.14	0.16	0.22	0.31	0.45	0.71
0.75	0.25	0.28	0.37	0.48	0.61	0.79
1.0	0.36	0.40	0.50	0.60	0.71	0.85

[a]From D. K. Trubey, *A Calculation of Radiation Penetration of Cylindrical Duct Walls*, ORNL-CF-63-2-64 (Feb. 28, 1963).

[b]Number of relaxation lengths.

such as a cosine distribution should be used at the artificial interface if t is greater than one relaxation length. Even when the original source is isotropic, the radiation will have taken on a more directional character after penetrating a relaxation length.

Simpler equations may be derived for the flux through partially penetrating ducts if the assumption is made that only the radiation penetrating the *end* of the partial duct need be considered. In this case the flux at P in Fig. 5.8*a* may be estimated by

$$\Phi \approx N_0[E_1(\mu t) - E_1(\mu t \sec \Psi)] , \qquad (5.40)$$

where $\Psi = \tan^{-1}[a/(Z - t)]$. Similarly, the flux at P due to radiation entering the mouth of a duct that penetrates only part of the shield but is adjacent

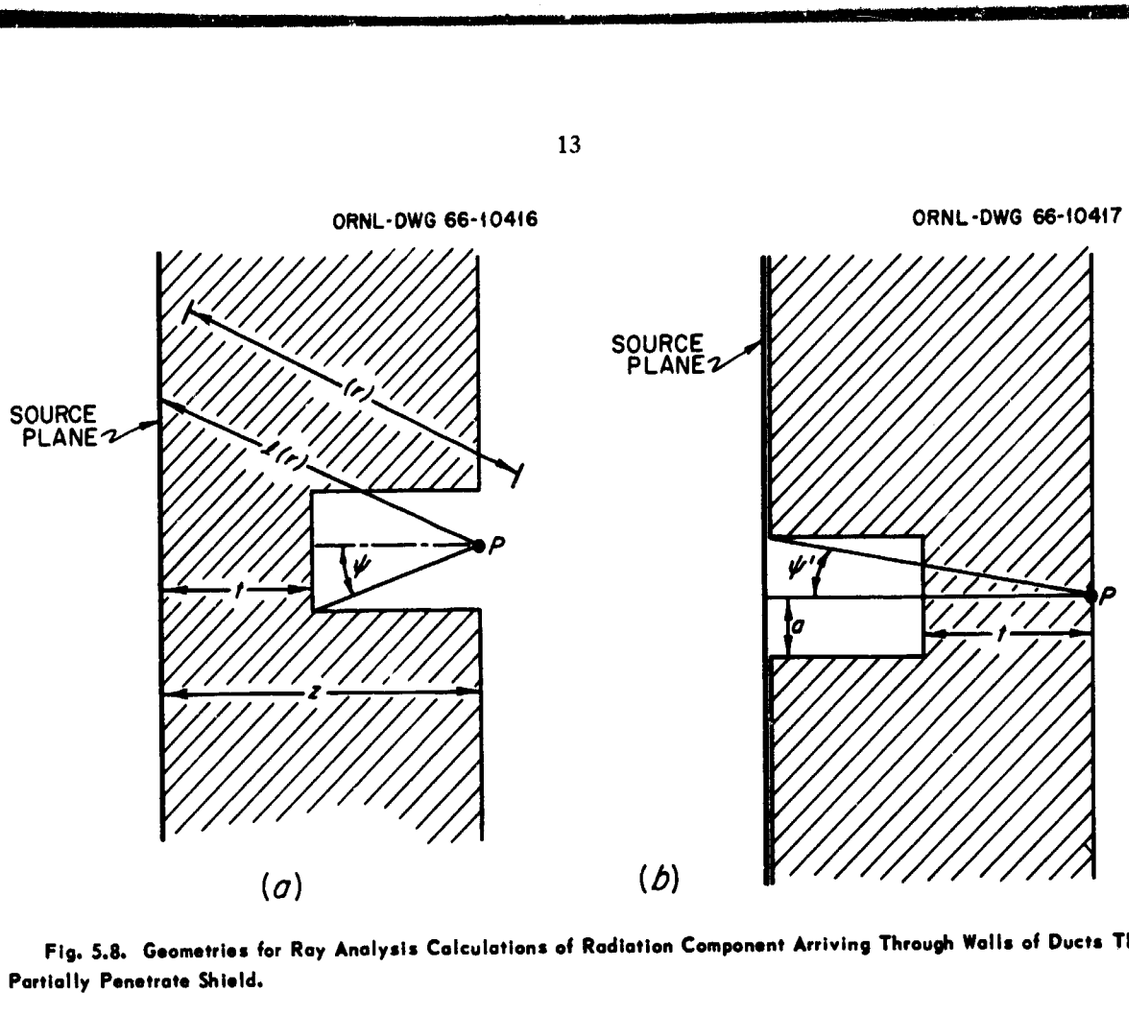

Fig. 5.8. Geometries for Ray Analysis Calculations of Radiation Component Arriving Through Walls of Ducts That Partially Penetrate Shield.

to the source (see Fig. 5.8*b*) is given by

$$\Phi = N_0[E_1(\mu t) - E_1(\mu t \sec \Psi')] , \qquad (5.41)$$

where $\Psi' = \tan^{-1}(a/Z)$.

For the same shield and duct dimensions, the angle Ψ' is smaller than Ψ and the peak flux increase at P due to the presence of the duct is greater in case *b* than in case *a*. For the approximation $\mu t \; a^2 \ll 2Z^2$, the integrated emergent current may be approximated by $\pi a^2 N_0 e^{-\mu t}[a^2/2(Z-t)^2]$ for either case *a* or *b*. Thus, while the peak current tends to be greater in case *b*, the integrated current increase due to the void is approximately the same in both cases.

Comparison with Experiment. – The ray analysis technique has been used successfully many times to predict experimental results for both gamma-ray and neutron transmission in solid unpenetrated shields. In complex geometries involving ducts, the technique should give better results for gamma rays than for neutrons, since neutrons on the average undergo more scatterings before they are absorbed or escape. However, as is demonstrated by the comparisons discussed below, the technique yields good results for the case of neutrons transmitted through straight ducts abutting a reactor.

The ray analysis technique was employed by Benenson and Fasano[6] to analyze experiments at the Brookhaven National Laboratory Shielding Facility on the transmission of fast neutrons through straight cylindrical ducts in a water shield. Neutrons from a fission source plate in the shielding facility entered the bottom of a water tank in which a duct had been vertically positioned and neutrons which reached the detector at the opposite end of the duct arrived there either through the base of the duct or through its walls after passing through the surrounding water. The ducts were 2, 4, 6, 8, 12, and 16 in. in diameter. The $^{32}S(n,p)^{32}P$ reaction was used to measure the fast-neutron flux, and an experimentally determined relaxation length was used to analyze the penetration of neutrons above the ^{32}S threshold from the fission source. Figure 5.9, which is typical of the results of this work, shows that the ray analysis method apparently yields good results when applied to streaming of very penetrating radiation from a diffuse source through simple ducts.

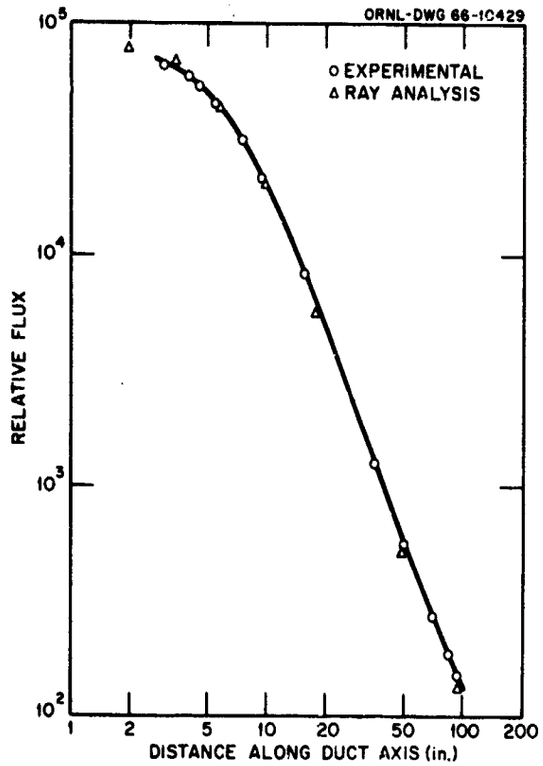

Fig. 5.9. Comparison of Ray Analysis Calculations with Measurements of Fast-Neutron Flux Along Axis of 8-in.-diam Straight Cylindrical Duct in a Water Shield: Fission Source at Duct Mouth. (From Benenson and Fasano, ref. 6.)

Piercey and Bendall[7] also used the ray analysis technique to calculate the flux of fast neutrons transmitted through straight cylindrical ducts. Their calculations corresponded to measurements made for 1-, 2-, and 3¾-in.-diam aluminum ducts positioned in the water of the LIDO Shielding Facility at Harwell, England. The duct lengths were up to 200 duct radii. As in the experiment discussed above, the fast flux was determined by the $^{32}S(n,p)^{32}P$ reaction. The calculations predicted the absolute sulfur reaction rate to within a factor of 2 over the experimental values. The poorest agreement occurred in the region of the duct nearest the reactor. It was concluded that most of the discrepancy resulted because of the inhomogeneity of the system and particularly because of the aluminum layer between the duct face and the reactor. Figure 5.10 shows a comparison of the calculated and experimental results as an example of this work.

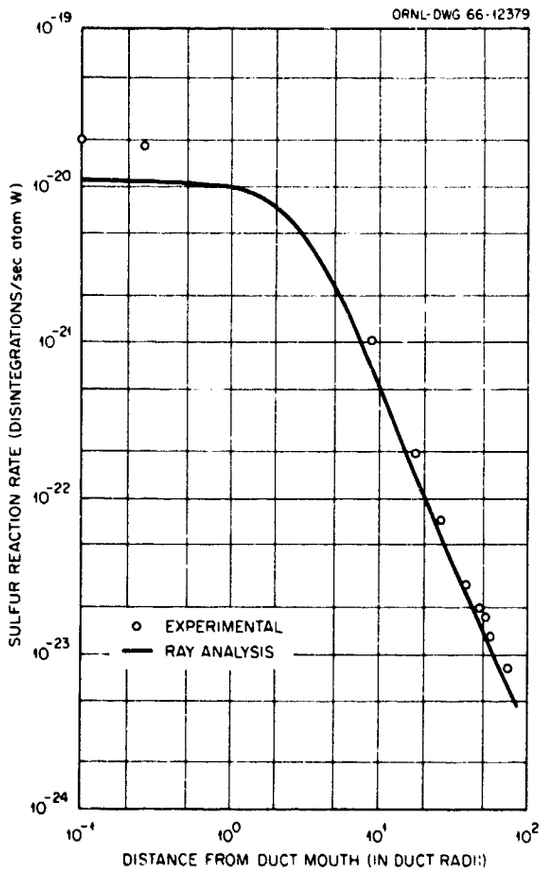

Fig. 5.10. Comparison of Ray Analysis Calculations with Measurements of Fast-Neutron Flux Along Axis of 3¾-in.-diam Straight Cylindrical Duct in a Water Shield: Duct Mouth Adjacent to Reactor Core. (From Piercey and Bendall, ref. 7.)

5.1.3. ANALOG MONTE CARLO METHOD

General Description. – It is shown in the preceding sections that for straight ducts in simple geometry the most important components contributing to the flux at the detector are the line-of-sight radiation and the radiation which enters the duct through its wall at the proper angle to reach the detector. For more complicated geometries involving ducts with bends, the line-of-sight component disappears and the dominant component becomes the radiation that is transmitted through the duct by successive scatterings from the surrounding shield material. Calculations of this contribution

require more sophisticated techniques than those described in the preceding discussion, since on the average many scatterings are involved and several boundaries are crossed.

A method that is potentially exact for calculating the radiation transmitted through a duct is the Monte Carlo method, often called "an experiment run on a computer." In general, the Monte Carlo method traces the path of a particle until, based on a probability distribution along the path, a collision occurs. The nature of this event is determined by selecting from a probability distribution of all possible interactions. If the event is an absorption, the history is generally terminated. If it is a scatter, direction and distance to the next collision are determined and the process is repeated until the particle is absorbed or until it exceeds the geometric or energy bounds of the problem. In most Monte Carlo programs there are wide variations in the statistical techniques, allowable events, and source-shield geometry which may be considered.

There are two types of Monte Carlo methods that can be applied to duct transmission problems: analog Monte Carlo methods, which are the methods referred to in this section, and albedo Monte Carlo methods, which are described in Section 5.4.4. The term "analog" is used to designate calculations in which the model solved is an analog of the interactions occurring as the particles traverse the duct and confining walls, as opposed to the albedo calculations in which the particles traversing a duct are followed by a random-walk process and wall interactions are represented by a reflection coefficient.

The analog Monte Carlo method is not always practical with the present programs and computing machinery because of the machine computing time required; nevertheless, several machine programs that have been developed are applicable to this type of calculation. Included among these are the ADONIS, LO5, COHORT, and O5R codes, all of which are described briefly in the appendix to this chapter.

Comparison with Experiment. – Collins and McCleary[8] used the LO5 Monte Carlo code to calculate the transmission of neutrons from a Po-Be source (3.08×10^7 neutrons/sec) through 12-in.-long, 3- and 6-in.-diam straight cylindrical ducts in water, with the detector positioned 3 in. from the duct mouth. The agreement that they obtained between the measured and calculated data, shown in Fig. 5.11, lends confidence in the ability of the LO5 procedure to predict neutron fluxes and dose rates beyond a straight cylindrical duct in a shield.

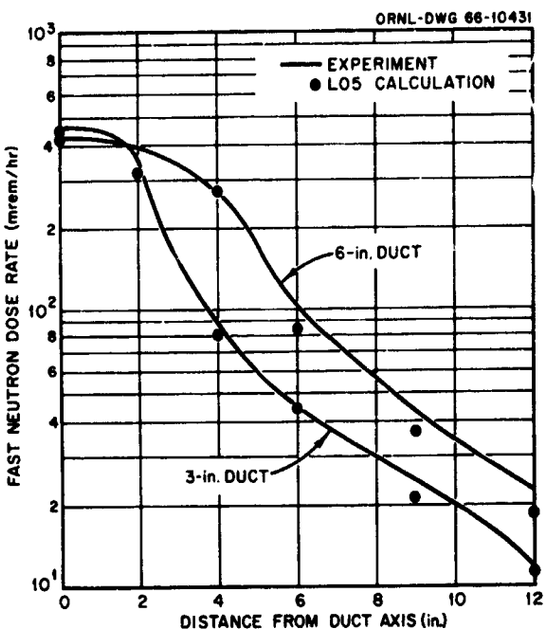

Fig. 5.11. Comparison of LO5 Analog Monte Carlo Calculations with Measurements of Fast-Neutron Dose Rates Along Axes of 12-in.-long 3- and 6-in.-diam Straight Cylindrical Ducts in Water: Po-Be Neutron Source. (From Collins and McCleary, ref. 8.)

The LO5 code was also used by Marshall[9] for calculations corresponding to measurements made of radiation transmitted through cylindrical ducts penetrating water shields. The ducts were constructed of 3-in.-diam aluminum tubing and had one bend midway along their lengths, with the bend angle varying between 30 and 60°. The sources were 14-MeV neutrons and ^{60}Co gamma rays positioned on the duct center line 3 in. from the mouth. The detector at the opposite end of the duct was also 3 in. from the duct mouth.

Figures 5.12 and 5.13 show a comparison of some typical experimental data and calculated results for the case of a 30° bent duct through an 18-in. water shield. In general, Marshall found that for shielding thicknesses which exceeded 18 in. the calculated dose rates were in good agreement with the experimental data in shape

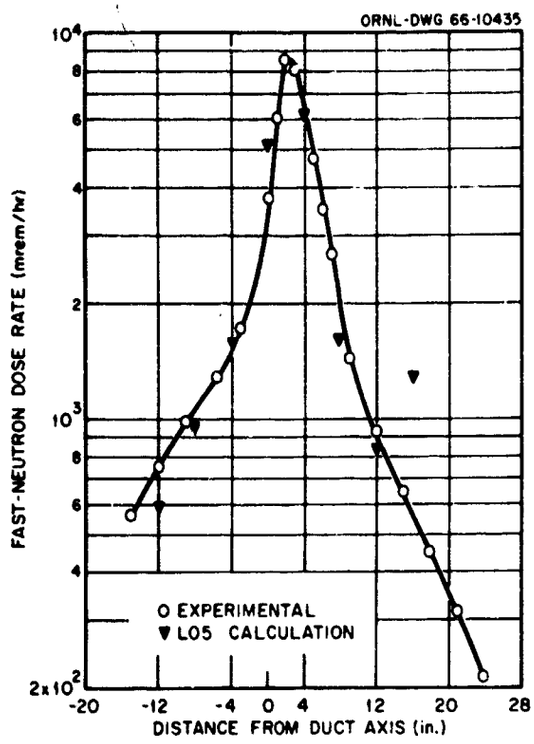

Fig. 5.12. Comparison of LO5 Analog Monte Carlo Calculations with Measurements of Fast-Neutron Dose Rate Transmitted Through 30° Bent Duct (3-in. diameter by 18 in.) in Water Shield: 14-MeV Neutron Source. (From Marshall, ref. 9.)

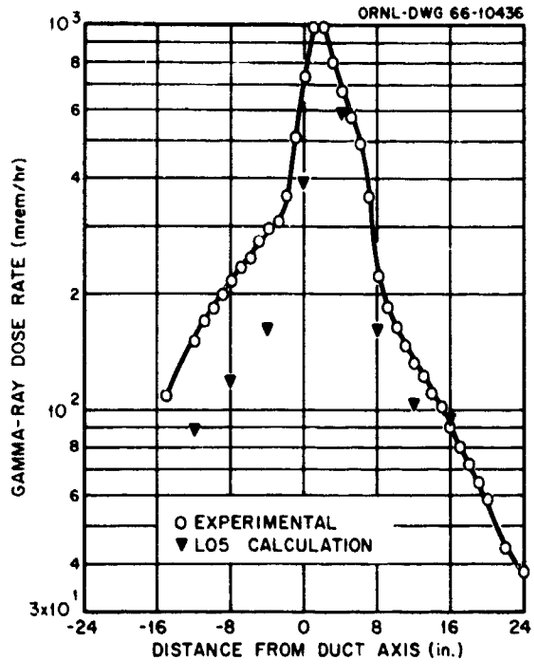

Fig. 5.13. Comparison of LO5 Analog Monte Carlo Calculations with Measurements of Gamma-Ray Dose Rate Transmitted Through 30° Bent Duct (3-in. diameter by 18 in.) in Water Shield: ^{60}Co Gamma-Ray Source. (From Marshall, ref. 9.)

but were too low in magnitude. He attributed this to three possible causes: the number of histories used in the calculations was insufficient, there was structure surrounding the experimental configuration that was not considered in the calculations, and there were errors in the cross-section values used.

Gardner and Mettler[10] used the ADONIS code[11] to predict the transmission of neutrons from a T(d,n) reaction source (14.7 MeV) through 11-in.- and 3-ft-square concrete ducts. They compared their results with measurements made by Doty[12] for an essentially isotropic source and with the albedo-type calculations made by Song[13] and by Maerker.[14] (Further discussion of the measurements and albedo calculations is give in Section 5.1.4.) Maerker's calculations were for lower source energies and there is some confusion in regard to the normalization of the various results, but since the correlations and results are preliminary in nature, Gardner and Mettler concluded that reasonably good agreement exists between the calculations and measurements. They also pointed out that the experimental measurements were subject to large error as a result of statistical variation of the measured dose rates, calibration of the instrument, and determination of the incident dose, and claimed only an order of magnitude accuracy.

Gardner and Mettler also used the ADONIS code to study the effect of the "corner lip" in multilegged rectangular ducts (see Section 5.1.4).

5.1.4. ALBEDO METHODS

General Description. – As is pointed out in Section 5.1.3, the primary means by which radiation is propagated through a duct with bends is by successive scatterings in the duct walls. The most practical way to evaluate this component is by using an albedo method. In general, this method assumes that the point at which radiation is incident on the duct wall is a point on an infinite

interface and that a certain fraction of the incident radiation will emerge from the wall at the same point. This fraction is called the albedo. In duct transmission calculations both total and differential albedos have been used. For best accuracy the albedos must be differential both in energy and in the angles of incidence and reflection.*

The simplest example of an albedo type of duct transmission calculation is one which considers radiation that has been reflected from a duct wall only once before reaching the detector. The calculation is performed by integrating a "reflection kernel" over the duct surfaces which have an unobstructed line of sight to both the source and the detector. Consider, for example, the case of a point source and simple duct shown in Fig. 5.14. The dose at P due to first-order reflection from the wall is

$$D = \int_{\substack{\text{wall}\\ \text{surface}}} \frac{N_p R(E_0)\, \alpha_{D2}(E_0,\theta_0,\theta,\phi) \cos\theta_0\, dS}{4\pi r_1^2 r_2^2}, \tag{5.42}$$

where

N_p = source strength,

E_0 = source energy,

$R(E_0)$ = flux-to-dose conversion factor,

$\alpha_{D2}(E_0,\theta_0,\theta,\phi)$ = differential dose albedo (reflected current per incident current),**

ϕ = azimuthal angle separating the incident and reflected rays,

and r_1, r_2, θ_0, and θ are defined in Fig. 5.14. The reflected dose must, of course, be added to the line-of-sight dose to obtain the total dose.

The Simon-Clifford equations[15] for neutrons reflected through ducts having cylindrical geometry (discussed later in this section) resulted from an integration of Eq. 5.42 for an assumed analytical fit to α. For cases in which a fit to their expression for α is possible, the Simon-Clifford equations should be used. Other fits may be derived

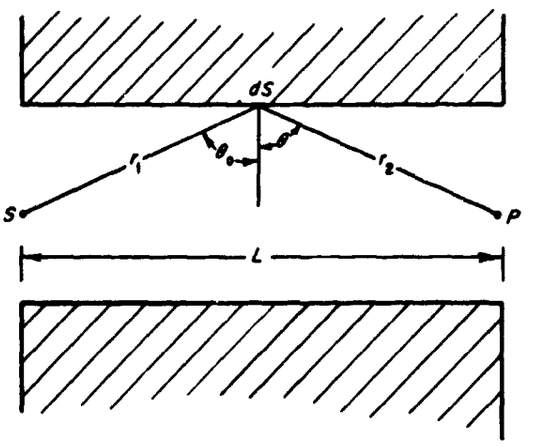

Fig. 5.14. Geometry for Albedo Calculation of Singly Reflected Radiation in a Simple Duct (Point Source).

which would allow the integration to be performed for simple geometries.

If either the nature of α or the geometry prohibits direct integration, Eq. 5.42 may be solved numerically by dividing the duct wall into small scattering areas and assuming that all points within an elemental scattering area are the same distance from the source or detector and that they have the same angles of incidence and reflection. A numerical evaluation performed by LeDoux and Chilton[16] led to a set of equations for calculating singly reflected gamma rays propagated through bent rectangular ducts. (The LeDoux-Chilton technique is discussed below.)

In the case of a broad-beam source incident on the duct at an angle, such as that shown in Fig. 5.15, no line-of-sight radiation reaches the detector and it is more important that all reflected radiation be evaluated, including that which has been reflected more than once. The singly reflected component at P is given by

$$D_{P_1} = \int_{\substack{\text{over}\\ \text{illuminated}\\ \text{area}}} \frac{D_i\, \alpha_{D2}(E_0,\theta_0,\theta,\phi) \cos\theta_0\, dS_1}{r^2}, \tag{5.43}$$

where D_i is the incident dose and r is the distance from the surface area element to the detector.

*Definitions of albedos and corresponding albedo data are presented in Chapter 4 of this Handbook.

**See the definitions given in Chapter 4; various other albedo forms may also be used.

The doubly reflected component is estimated by

$$D_{P_2} = \int_{\substack{\text{over} \\ \text{illuminated} \\ \text{area}}} \int_{\substack{\text{all} \\ \text{area}}} \frac{D_i \, \alpha_{D2}(E_0,\theta_0,\theta,\phi_1) \cos\theta_0 \, dS_1 \, \alpha_{D2}(E_1,\theta_1,\theta_2,\phi_2) \cos\theta_1 \, dS_2}{r_1^2 r_2^2} . \quad (5.44)$$

Complexities of the problem will almost always require the use of a computer program for numerical evaluation of these equations. Cain[17] has shown that for the case of low-energy neutrons, numerical evaluation of these integrals becomes impractical because the number of reflection events which must be considered in order to adequately calculate the penetrating radiation is so large. As an alternative, a method was developed that traces particles through successive reflection events by a Monte Carlo technique which uses a random-walk process to avoid excessive run-time penalties associated with the usual Monte Carlo calculation. This method is discussed later in this section.

In most albedo calculations of the transmission of radiation through rectangular ducts with bends, the corner lip (the corner formed by the intersection of two legs) is assumed to be opaque to radiation in the main parts of the calculation and a correction is made for its effect with a separate approximate calculation. This correction is usually broken down into two contributions: the corner-lip transmission effect and the corner-lip inscattering effect.

ORNL-DWG 66-10410

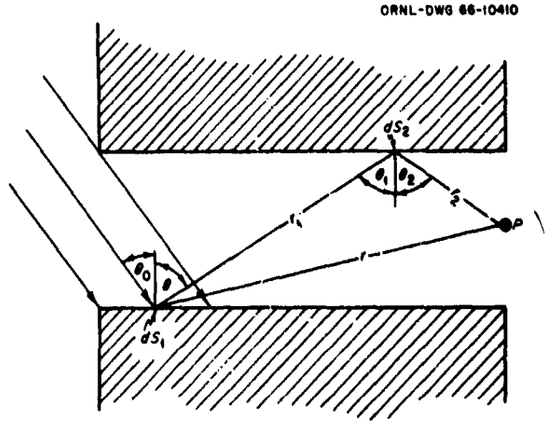

Fig. 5.15. Geometry for Albedo Calculation of Doubly Reflected Radiation in a Simple Duct (Broad-Beam Source).

The corner-lip transmission effect is illustrated in Fig. 5.16 by the dashed line that originates at the duct entrance and passes through the inside corner. The radiation penetrating the lip scatters from the opposite wall and contributes to the dose at the detector. In accounting for this radiation, the albedo integrations of Eqs. 5.43 and 5.44 can be performed, with the incident dose represented by a variable which depends on the path length in the duct wall material of a ray that is parallel to the initial direction of the radiation and terminates at the scattering point. An approximation may be made by assuming that all particles which penetrate the material with a path length less than a relaxation length are unattenuated and that all particles which penetrate more than a relaxation length are completely absorbed. (LeDoux and Chilton used the energy absorption coefficient to

ORNL-DWG 66-10415

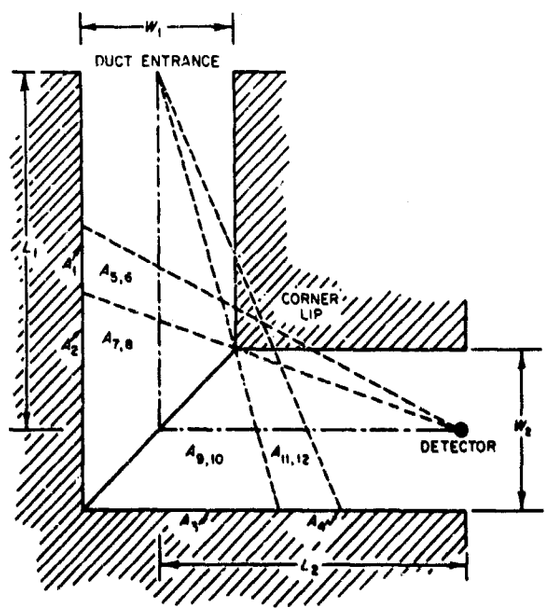

Fig. 5.16. Geometry for Determining Corner-Lip Transmission Effect in Two-Legged Rectangular Duct. This geometry is also used in the illustration of the LeDoux-Chilton technique discussed later in this section.

ORNL-DWG 66-10430

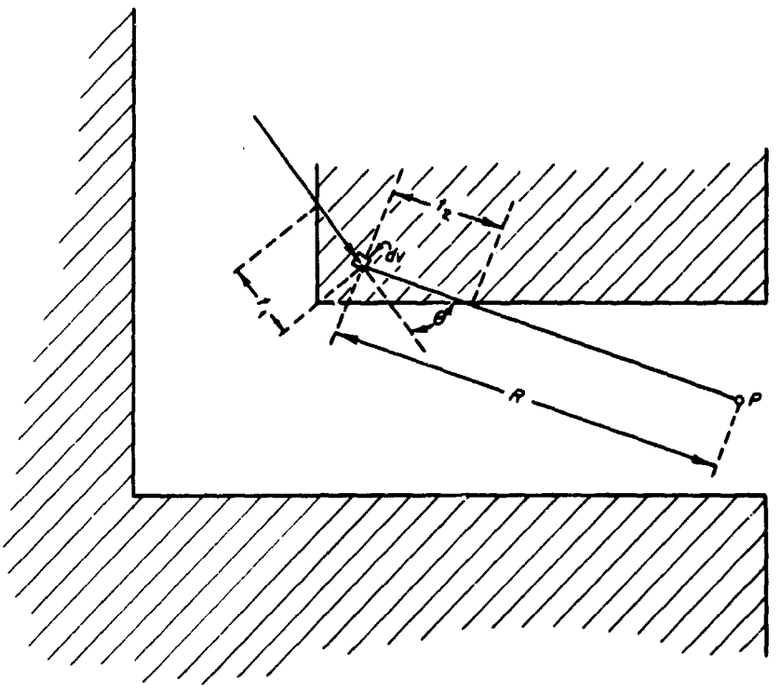

Fig. 5.17. Geometry for Last-Collision Calculation of Corner-Lip Inscattering Effect in Two-Legged Rectangular Duct.

estimate this effective relaxation length for gamma rays.) On this basis, the effect of the comer-lip penetration can be approximated by an increase in the number of scattering areas beyond the primary scattering areas. The areas designated as A_1, A_4, A_5, A_6, A_{11}, and A_{12} in Fig. 5.16 show some of these additional scattering surfaces.*

The comer-lip inscattering effect results in some of the radiation being redirected toward the detector by scattering in the corner lip. This component may be evaluated by using a last-collision[16] technique, for which the geometry is shown in Fig. 5.17. The flux at a distance t_1 in the corner lip is given by

$$\Phi(t_1) = \Phi_0 \exp\left[-\frac{t_1}{\lambda(E_0)}\right], \qquad (5.45)$$

where $\lambda(E_0)$ is the effective relaxation length for the incident radiation in the material. The radiation per unit solid angle scattering toward P by the ith element in the material is given by $\Phi K_i(E,\theta) N_i\, dv$, where $K_i(E,\theta)$ is the differential angular scattering cross section of material i for radiation incident at energy E, and N_i is the atomic density of element i in the duct wall material. The flux at P due to radiation of energy E scattering in the lip is then

$$\Phi = \int_{\substack{\text{over}\\ \text{scattering}\\ \text{volume}}} \left\{ dv\, \Phi_0\, e^{-[t_1/\lambda(E_0)]} \right\} \sum_i K_i(E_0,\theta) \times N_i \left\{ e^{-[t_2/\lambda(E_1)]} \right\} \frac{1}{R^2}, \qquad (5.46)$$

where E_1 is the energy after scattering. This technique is analogous to integrating a point kernel over the scattering volume, with the strength of the source point used as the differential scattering density at that point.

*In the ADONIS Monte Carlo calculations reported in Section 5.1.3, Gardner and Mettler[10] included a study of the comer-lip effect by performing two calculations which utilized different importance functions. By proper selection of the weighting functions it was possible to eliminate most of the corner-lip penetration or to allow for the penetration. It was shown that the comer-lip effect can be important for some conditions.

Simon-Clifford Technique for Cylindrical Ducts. – The albedo method of Simon and Clifford[15] is one of the least complicated of the methods available for calculating the transmission of thermal and intermediate-energy neutrons through cylindrical ducts. It considers only the neutrons entering the open end of the duct, and transmission is assumed to be either by line of sight or by scattering from the duct walls. The wall scattering is calculated by using a single-energy "spectrum-averaged" material albedo.

In the case of a straight cylindrical duct, the albedo, A_2, is defined as the fraction of incident neutrons which are reradiated (see Chapter 4). In this form of the albedo, the reflected radiation has been integrated over all exit directions, the reflected angular distribution being expressed in the general form $\beta + (2\gamma \cos \theta)/2\pi$, where β is the fraction reradiated isotropically, γ is the fraction reradiated with a cosine distribution, and $\beta + \gamma = 1$. The flux at distance Z along a duct of radius a is then given by

$$\Phi(Z) = \frac{N_0}{2}\left(\frac{a}{Z}\right)^2\left[1 + \left(\frac{A_2}{1 - A_2}\right)\left(\beta + \frac{4\gamma a}{Z}\right)\right], \quad (5.47)$$

where $\Phi(Z)$ is in the same units as the surface source strength N_0.

The first term in this equation is the line-of-sight component given in Section 5.1.1. The second term, which accounts for the wall-scattering component, is a strong function of the material albedo. Since A_2 is of the order of 0.1 for fast neutrons and the second term is small for long thin ducts ($a \ll Z$), Eq. 5.47 simplifies to that for the uncollided flux. However, for thermal neutrons, which have an albedo of about 0.8, the second term becomes important, and the scattered flux can dominate.

This approach[15] was extended to cover the case of a bent cylindrical duct (see Fig. 5.18) by assuming that the albedo (in the area of the bend) of the neutrons transmitted through the first leg of the duct is the source for calculation of transmission through the second leg. When both legs are of equal diameter and their angular separation is θ, the total transmission at a distance Z_2 along the second leg is given by

$$\Phi(Z_2) = \frac{N_0 A_2'}{4}\left(\frac{a}{L_1}\right)^2\left(\frac{a}{Z_2}\right)^2\left(\frac{\beta + 2\gamma \sin \theta}{\sin \theta}\right), \quad (5.48)$$

ORNL-DWG 66-10403

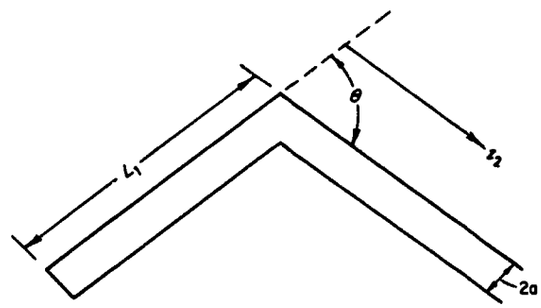

Fig. 5.18. Geometry for Calculating Neutron Transmission Through Cylindrical Duct by Simon-Clifford Method.

where A_2' is an empirically determined albedo parameter.

If a series of bends are involved, the flux at a distance Z from the last bend may be expressed as

$$\Phi(Z_n) = \frac{N_0}{2}\left(\frac{a}{Z_n}\right)^2\left[A_2'\left(\frac{a}{L_1}\right)^2\left(\frac{\beta + 2\gamma \sin \theta_1}{\sin \theta_1}\right)\right] \cdots \left[A_2'\left(\frac{a}{L_{n-1}}\right)^2\left(\frac{\beta + 2\gamma \sin \theta_{n-1}}{\sin \theta_{n-1}}\right)\right], \quad (5.49)$$

where the duct segments are of lengths $L_1, L_2, \ldots L_n$ and are separated by angles $\theta_1, \theta_2, \ldots \theta_{n-1}$.

Ducts which follow a smooth curve through the shield may be treated by the above method provided that the radius of curvature is large with respect to the radius of the duct.[3] The curved path may be divided into a series of equivalent straight sections of length equal to the maximum chord which can be drawn internal to the duct. The angular separation between successive chords may then be used as the angle between the equivalent sections.

Horton[19] treated the case of helical ducts with an albedo approach similar to the Simon-Clifford method. For a helical path divided into n equivalent straight sections of radius a and length l deviating successively by constant angle ψ, the flux is approximated by

$$F = \frac{N_0}{2^n}\left(\frac{a}{l}\right)^{2n}(A_2' \operatorname{cosec} \psi)^{n-1}. \quad (5.50)$$

This may be compared with Eq. 5.49 which would be the equivalent Simon-Clifford expression provided that all values of θ equal ψ and all values of L equal l.

The usefulness of the semiempirical albedo techniques described above depends on the availability of suitable values of the albedos and angular distributions of the reflected neutrons.

LeDoux-Chilton Technique for Rectangular Ducts. A method of calculating gamma-ray transmission through two-legged rectangular ducts was formulated by LeDoux and Chilton,[16] and the same general technique was used by Song[13] for neutron transmission. Equations were derived for calculating radiation streaming down two-legged concrete ducts using as transport mechanisms: (1) a single-reflection albedo for surfaces that can be "seen" by both the source and the detector, and (2) scattering by material in the corner lip of the duct.

In the absence of sufficient differential albedo data at the time of this work, a total albedo[20] was used and the radiation was assumed to emerge isotropically. To simplify the equations, it was assumed that all points on a major scattering area (numbered areas of Fig. 5.16) could be considered to have the same angle of incidence from the source and the same reflection angle to the detector. Formulas were then derived for the detector response due to the first-order scattering from each of the surfaces. Later work[21–23] with more accurate differential albedo data showed that this method tends to underpredict because multiple reflections are neglected. That the method predicts experimental data as well as it does is attributed to a compensating overprediction caused by the assumption of isotropic scattering.

Chapman[24] extended the LeDoux-Chilton approach to include double reflections and second-order effects such as a wall backscatter followed by a corner-lip inscatter. In place of the total albedos with the assumption of isotropy of the reflected radiation used by LeDoux and Chilton, Chapman substituted the semiempirical formula for the differential dose albedo that was derived by Chilton and Huddleston[25] (see Section 5.1.5). The two parameters in this formula were determined by a least-squares fit to the Monte Carlo data of Raso.[23]

The complexity of the interaction combinations considered (e.g., one backscatter, one inscatter, one backscatter plus one penetration, two backscatters, and one backscatter plus one inscatter) dictated that Chapman use four computer programs to calculate the following:

1. the original LeDoux-Chilton formulas (singly reflected component),
2. the LeDoux-Chilton formulas with the scattering areas broken into smaller increments,
3. the contribution due to second-order scattering from the duct walls,
4. the contribution due to inscatter by the corner lip of the duct of either direct or first-order wall-scattered radiation.

The singly reflected component was evaluated by integrating over each of the numbered areas in Fig. 5.16. In evaluating penetration through the corner lip, the assumption was made that rays penetrating less than one relaxation length of material are unattenuated and that those encountering more than one relaxation length of material do not penetrate. Scattering in the corner lip was calculated using the singly reflected formula which LeDoux and Chilton derived on the basis of Klein-Nishina differential scattering probabilities.

To perform the double-reflection calculations, Chapman divided the duct into a larger mesh consisting of 12 scattering areas as shown in Fig. 5.19, and combinations which would allow transport from the source to the detector with two scatters were considered. Combinations whose percentage

ORNL-DWG 66-10411

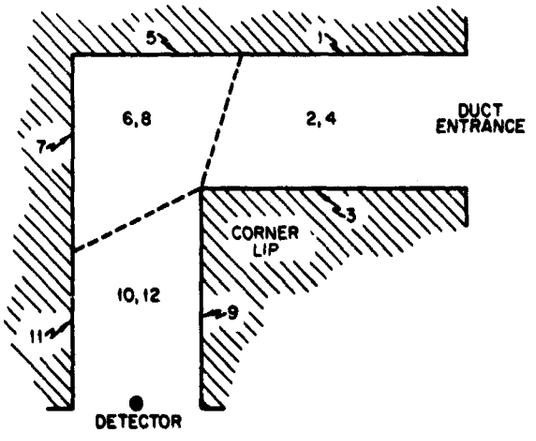

Fig. 5.19. Scattering Areas for Albedo Calculation of Doubly Reflected Gamma Rays in Two-Legged Rectangular Duct.

contribution to the total dose was considered to be small were deleted. Specifically these were reflection from surface 1 to surfaces 10 and 12 and reflection from surfaces 2 and 4 to surfaces 10, 11, and 12. The incidence of singly reflected radiation on the corner lip of the duct was combined with the lip inscatter calculation to determine the contribution due to one backscatter plus one inscatter. In all cases the energy degradation in a reflection was assumed to be that of a single Compton scattering.

In calculating neutron transmission through rectangular ducts, Song[13] used Chapman's modification of the LeDoux-Chilton method with the exception that the reflected neutron spectrum was assumed to consist of two neutron energy groups, the number and energy in each group being based on the Monte Carlo data of Allen, Futterer, and Wright.[26] Song derived a semiempirical formula for use in the calculations in terms of a single-energy parameter for the differential neutron dose albedo in a manner analogous to that used by Chilton and Huddleston[25] in their gamma-ray calculations. Values for the energy-dependent parameter were obtained by a least-squares analysis that gave the best fit to the data of Allen *et al.*

Monte Carlo Methods for Rectangular Ducts. – Generally, experiments and calculations have shown that gamma rays produced by neutron absorptions in a concrete shield surrounding a rectangular duct make a significant contribution to the total dose in the duct, and analysis of this component requires a knowledge of the distribution of low-energy neutrons throughout both the duct and the shield. These distributions can be determined exactly by analog Monte Carlo calculations, but, as was pointed out in Section 5.1.3, the machine time required to trace neutrons until they approach thermal equilibrium can become excessive. To circumvent this, Cain developed a technique[17] that uses a random-walk Monte Carlo approach in which particles are traced by selecting random path directions inside the duct while prohibiting particle penetration into the shielding material. Thus, tracking through the large number of interactions prior to emergence from the wall material is averted and no time is wasted in tracking particles which never emerge. Each time a particle encounters the wall, it is assumed to re-emerge with a reduced weight, given by the incident weight times the albedo of the wall. Fluxes at various points along the duct are then calculated either by making a statistical estimate from each encounter to point detectors or by determining the track length per unit volume in a detector region. The most satisfactory detector was found to be a thin region extending across the duct and perpendicular to the duct axis.

The method was modified by Maerker and Cain[27] to include doubly differential thermal-neutron current and fast-neutron dose albedo data (differential in reflected solid angle and energy) previously determined[28–30] by Monte Carlo calculations for infinite slabs of concrete (see Chapter 4). In addition, a provision was included to calculate the capture-gamma-ray dose rate arising from neutron capture in the duct walls.

In the modified code the incident neutrons are reflected with reduced "weight" into various energy groups and directions, the probabilities for which are predetermined from the doubly differential albedo data. The neutrons are followed in the random-walk procedure until they either escape out the front or rear end of the duct or are killed by Russian roulette when their weight falls below a predetermined value. Statistical estimations of the fluxes to point detectors are made to obtain the results.

The best accuracy is obtained when the calculations are done separately for three energy ranges: (1) Neutrons with energies from 200 keV to 8 MeV are divided into six energy groups and are sampled to obtain the fast flux contribution to the dose rate. (2) The dose rate from neutrons of intermediate energy (0.5 eV to 200 keV), including all neutrons that have slowed down to intermediate and thermal energies from higher energy groups, is determined with a 13-group calculation that involves sampling the entire energy range from thermal to 8 MeV but scoring only those neutrons with energies below 200 keV. (3) The dose rate from source thermal neutrons (subcadmium, <0.5 eV) is then determined in a separate calculation using a single-velocity model.

Different Monte Carlo albedo data are used in each energy range. The albedos used for the fast-neutron calculation are those reported for concrete by Maerker and Muckenthaler;[28] they do not cover neutrons reflected with energies less than 200 keV. The albedos used for the intermediate-energy neutrons are those determined by Coleman *et al.*[29] The latter include the probability of higher energy neutrons being reflected as thermal neutrons. The albedos for neutrons that have thermal energy both

before and following reflection are those determined by Maerker and Muckenthaler[30] using a one-velocity model. Finally, the equivalent of an albedo is used to calculate the capture-gamma-ray contribution to the dose, the results being correlated on the basis of the gamma-ray dose emitted per steradian per incident neutron at a particular angle of incidence and within a certain energy group. The capture-gamma-ray albedos for incident thermal neutrons were developed by Maerker and Muckenthaler[30] and those for incident intermediate neutrons by Coleman *et al.*[29]

In this modified method no neutron is allowed to penetrate a corner wall during the course of its random walk, although a statistical estimate of the flux that includes a corner-lip penetration in the last flight may be made. This is accomplished simply by neglecting the contribution when the path through a corner is greater than 1 mean free path and including the unattenuated contribution if the path is less than 1 mean free path. No consideration is given to the corner-lip inscattering effect.

Comparison with Experiment. – The accuracy of albedo-type duct streaming calculations depends on the accuracy of the albedo data used, on the detail with which the scattering surface mesh and the energy groups are defined, and on the selection of the multiply scattered components to be included. The comparisons given in the following paragraphs show the extent of agreement that has been obtained when the albedo approach has been used to analyze a variety of experiments. The reason that most of the comparisons are for gamma rays from isotope sources attenuated through bent rectangular ducts is that a number of experiments have been performed with such sources in conjunction with studies on the design and evaluation of shelters to protect against fallout radiation. Only typical data have been selected for the comparisons presented here, since an exhaustive summary has been published by Huddleston and Wilcoxson.[31]

Comparisons with 51 different measurements were made by Chapman,[24] who used the extended LeDoux-Chilton technique to calculate gamma-ray dose rates at the exit end of two-legged L-shaped rectangular ducts, the source in each case being a gamma-ray-emitting isotope at the mouth of the duct. The results are presented in Table 5.4, where W, L_1, and L_2 are as defined in Fig. 5.16. Agreement is generally within 30% for a ^{60}Co or ^{24}Na source, within 45% for ^{137}Cs, and within a factor of 2 for ^{198}Au. The analysis overpredicted the experimental results fairly consistently, but not by a consistent margin.

Chapman also calculated the gamma-ray dose rates along the axes of two- and three-legged rectangular ducts and some of them are compared in Figs. 5.20 through 5.23 with the dose rates measured at several points along the duct axes for three sources of different energy.[32–34] Figures 5.21 and 5.22 also show comparisons with a simplified formula (Eq. 5.51) proposed by Ingold and Huddleston,[35] which is discussed in Section 5.1.5.

As is apparent from Table 5.4, a number of the experiments with which Chapman made his comparisons were performed by Terrell *et al.*[32–34] Although not considered by Chapman in his comparisons, some of the experiments performed by Terrell *et al.*[32] were to investigate the effect of geometry and source energy on the attenuation of gamma rays through rectangular concrete ducts with two right-angle bends, the results of which show trends which can be anticipated in calculations. They found that for 6-ft-square concrete ducts it made little difference whether the gamma-ray source was ^{60}Co or ^{137}Cs or whether the right-angle bends formed a U shape (Fig. 5.24*a*) or a Z shape (Fig. 5.24*b*). These data, plotted in Fig. 5.24c, show a maximum deviation of a factor of 1.5 when properly normalized. The effect of geometry and energy becomes more noticeable in the case of a 1-ft-square duct. Typical examples of the effect of gamma source energy and duct shape are shown in Figs. 5.25 and 5.26 respectively.

In his studies Chapman also calculated the contribution of a given scattering area on the gamma-ray dose rate in an L-shaped 3-ft-square concrete duct.[36] The scattering area chosen was the one shown as S_1 in Fig. 5.27*a*, it being assumed that gamma rays from a ^{60}Co source at the mouth of the duct were scattered from this area to the detector at the exit end of the duct. The dose rate due to gamma rays initially scattered from S_1 was calculated to be 0.379 mr/hr, which compares quite favorably with a measured dose rate of 0.404 mr/hr.

During the experiment, Chapman measured the gamma-ray spectrum at the exit end of the duct both with and without the scattering area S_1 being shadowed from the source. The results are shown in Fig. 5.27*b*. Shielding of S_1 had a more pronounced

Table 5.4. Comparison of Gamma-Ray Dose Rates Predicted by LeDoux-Chilton Technique with Dose Rates Measured at Exit End of Two-Legged Duct[a]

Gamma-Ray Source	W	L_1/W	L_2/W	Dose Rate (mr/hr)		% Difference[b]	Reference
				Calculated	Measured		
0.34-curie ^{60}Co	11 in.	1.90	1.65	87.3	125	−30	Green[c]
			2.06	44.5	61	−27	
			2.46	27.1	30.5	−11	
			3.68	8.46	7.31	+16	
		3.58	2.06	6.17	7.3	−15	
			2.86	2.61	2.7	−3	
			3.68	1.30	1.3	0	
0.6-curie ^{60}Co	11.1 in.	3.54	1.73	17.4	15.6	+11	Eisenhauer[d]
			2.79	4.94	3.7	+33	
			3.51	2.65	2.02	+31	
55-curie ^{60}Co	12 in.	3.50	2.0	916	852	+8	Terrell[e]
			3.0	317	243	+30	
			4.0	140	110	+28	
2.4-curie ^{60}Co	3 ft	2.0	1.67	20.6	17.5	+18	Chapman[f]
			2.0	12.6	12.1	+4	
			2.34	8.35	7.1	+18	
		2.5	1.50	14.5	13.5	+7	
			1.83	8.42	9.1	−8	
			2.0	6.70	6.4	+5	
			2.5	3.79	3.7	+2	
3.67-curie ^{60}Co	6 ft	1.33	1.83	15.4	11.8	+31	Terrell[g]
			2.50	6.56	4.75	+38	
			3.17	3.47	2.42	+43	
		1.66	1.83	7.85	7.30	+8	
			2.50	3.46	2.73	+27	
			3.17	1.85	1.39	+33	
		2.0	1.83	4.71	4.56	+3	
			2.50	2.12	1.79	+18	
			3.17	1.14	0.935	+21	
80-curie ^{137}Cs	12 in.	3.5	2.0	606	430	+41	Terrell[e]
			3.0	208	132	+58	
			4.0	90	90	+41	
	6 ft	2.17	1.83	36.5	35.5	+3	
			2.33	19.7	19.6	0	
1.52-curie ^{137}Cs	6 ft	2.0	1.83	0.858	0.714	+20	
			3.17	0.207	0.186	+11	
15.5-curie ^{198}Au	3 ft	2.0	1.67	55.8	37.6	+48	Chapman[h]
			2.0	34	23.3	+46	
			2.67	15.7	11.1	+41	
	11 in.	4.125	2.04	85	46.7	+83	
			2.86	35.2	19.0	+85	
			3.27	24	13.5	+78	

Table 5.4 (continued)

Gamma-Ray Source	W	L_1/W	L_2/W	Dose Rate (mr/hr)		% Difference[b]	Reference
				Calculated	Measured		
4.2-curie ^{24}Na	6 ft	1.66	1.83	8.77[i]	6.78	+29	Terrell[j]
			2.50	3.84	2.80	+37	
			3.17	2.05	1.50	+37	
		2.17	1.83	4.17	3.64	+15	
			2.50	1.88	1.67	+13	
			3.17	1.02	0.912	+11	
		2.84	1.83	2.02	1.94	+9	
			2.50	0.931	0.828	+12	
			3.17	0.475	0.462	+3	

[a]Table taken from: J. M. Chapman, *Computer Calculations of Dose Rates in Two-Legged Ducts Using the Albedo Concept*, Naval Civil Engineering Laboratory Report NCEL-R-264 (Oct. 24, 1963).

[b]Percent difference = (calculated − measured/measured) 100.

[c]D. W. Green, *Attenuation of Gamma Radiation in a Two-Legged 11-inch Rectangular Duct*, Naval Civil Engineering Laboratory Report NCEL-R-195 (May 2, 1962).

[d]C. Eisenhauer, *Scattering of Cobalt-60 Gamma Radiation in Air Ducts*, National Bureau of Standards Technical Note 74 (1960).

[e]C. W. Terrell, A. J. Jerri, and R. O. Lyday, Jr., *Radiation Streaming in Ducts and Shelter Entranceways*, Armour Research Foundation Report ARF 1158-AO2-7 (April 1962).

[f]J. M. Chapman, *Gamma Dose Rates and Energy Spectra in a 3-Foot Square Duct*, Naval Civil Engineering Laboratory Report NCEL-N-443 (June 1962).

[g]C. W. Terrell *et al.*, *Radiation Streaming in Shelter Entranceways*, Armour Research Foundation Report ARF 1158-12 (October 1960).

[h]J. M. Chapman, *The Variation of Dose Attenuation of Two-Legged Concrete Ducts with Incident Gamma-Ray Energy*, Naval Civil Engineering Laboratory Report NCEL-TN-707 (April 1965).

[i]The values for ^{24}Na are the sum of the values obtained using initial gamma-ray energies of 1.37 and 2.75 MeV.

[j]C. W. Terrell and A. J. Jerri, *Radiation Streaming in Shelter Entranceways*, Armour Research Foundation Report ARF 1158-AO1-5 (July 1961).

effect on the higher energy radiation than on the multiply reflected low-energy component. This effect would be expected since the percentage reduction in the single-reflected area that results from blocking S_1 is greater than the percentage reduction in possible combinations of multiple-reflection areas.

In a subsequent experiment, Chapman and Grant[37] investigated the relative effectiveness of coplanar and noncoplanar three-legged rectangular ducts. For the cases investigated (11-in.-square duct, ^{60}Co source, L_1 = 30 in., L_2 = 31.5 in., L_3 = 36 in.), the attenuation provided by the noncoplanar configuration was found to be greater by a factor of 2 than that provided by the coplanar case. This effect cannot be explained by analysis because third or higher order reflections are difficult to treat with the albedo theory. The difference could be due to geometric effects on the scattering angles.

Clifford[21] used differential albedos[23] to calculate dose rates corresponding to those measured in experiments designed to determine the importance of multiple reflection on the transmission of ^{137}Cs gamma rays through 8-in.-, 12-in.-, and 3-ft-square concrete ducts. In the experiments, collimated gamma rays were incident on the duct entrance at an angle to the duct axis such that the area in which the first reflection could occur was near the entrance of the duct (see Fig. 5.28a). The dose rate along the duct center lines was first measured with the concrete duct unmodified (Condition *A*) and then, in order to estimate the influence of each reflection area in the duct, with a lead lining covering all inside surfaces of the duct except the first-scatter area (Condition *B*)

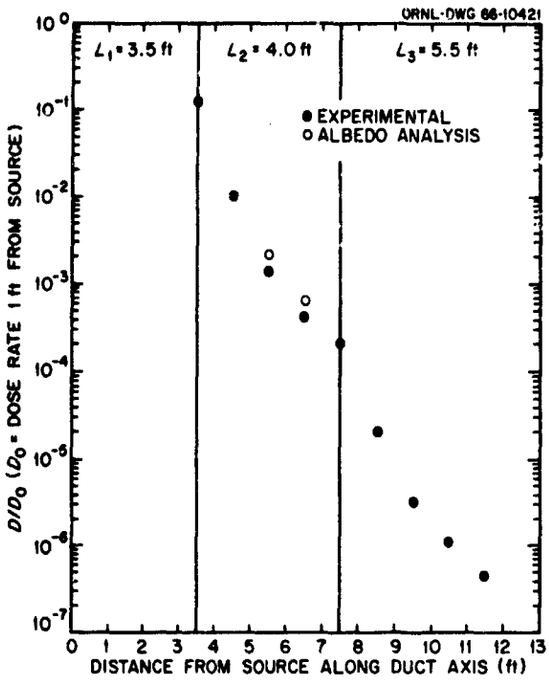

Fig. 5.20. Comparison of Albedo Calculations with Measurements of Gamma-Ray Dose Rates Along Axis of 1-ft-square U-Shaped Concrete Duct: 80-curie ^{137}Cs Gamma-Ray Source. (Experimental data from Terrell *et al.*, ref. 32; calculations from Chapman, ref. 24.)

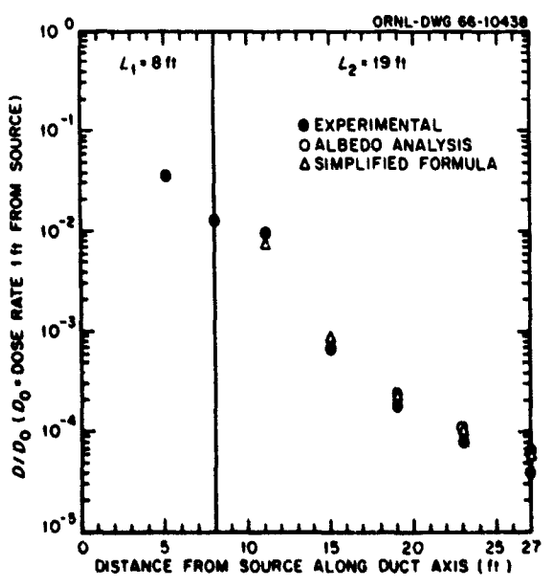

Fig. 5.22. Comparison of Albedo Calculations with Measurements of Gamma-Ray Dose Rates Along Axis of 6-ft-square L-Shaped Concrete Duct: 3.67-curie ^{60}Co Source. The results designated "simplified formula" correspond to the Ingold-Huddleston equation given in Section 5.1.5. (Experimental data from Terrell *et al.*, ref. 33; calculations from Chapman, ref. 24.)

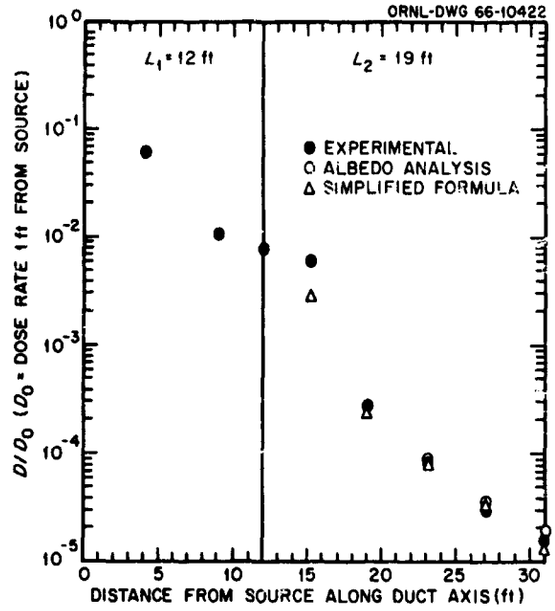

Fig. 5.21. Comparison of Albedo Calculations with Measurements of Gamma-Ray Dose Rates Along Axis of 6-ft-square L-Shaped Duct: 3.67-curie ^{60}Co Source. The results designated "simplified formula" correspond to the Ingold-Huddleston equation given in Section 5.1.5. (Experimental data from Terrell *et al.*, ref. 33; calculations from Chapman, ref. 24.)

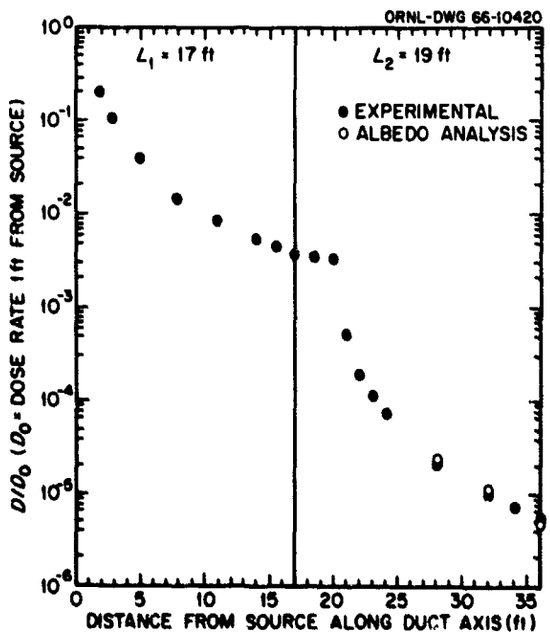

Fig. 5.23. Comparison of Albedo Calculations with Measurements of Gamma-Ray Dose Rates Along Axis of 6-ft-square L-Shaped Duct: 4.2-curie ^{24}Na Source. (Experimental data from Terrell *et al.*, ref. 34; calculations from Chapman, ref. 24.)

ORNL-DWG 66-10433

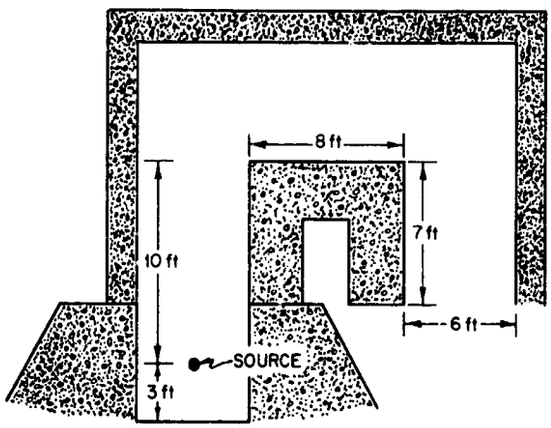

Fig. 5.24*a*. Geometry of U-Shaped Duct.

ORNL-DWG 66-10432

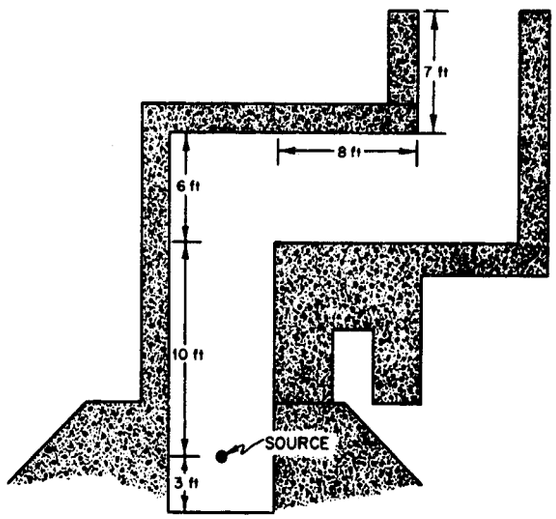

Fig. 5.24*b*. Geometry of Z-Shaped Duct.

ORNL-DWG 66-10419

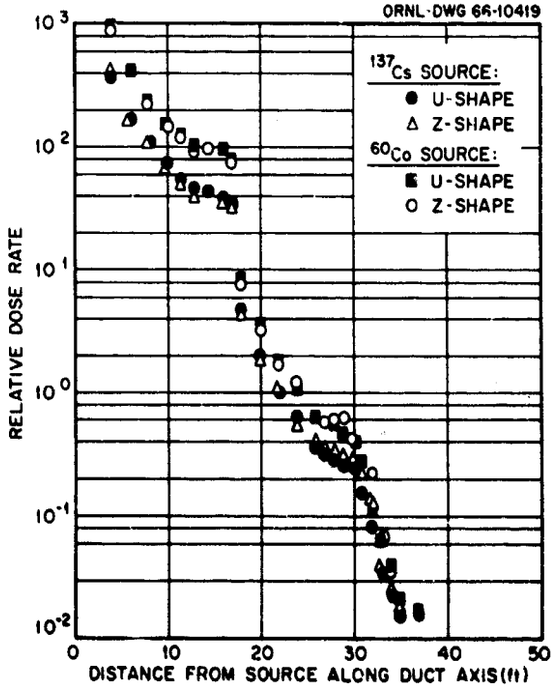

Fig. 5.24*c*. Gamma-Ray Dose Rates Measured in 6-ft-square U- and Z-Shaped Concrete Ducts: ^{60}Co and ^{137}Cs Gamma-Ray Sources. (From Terrell *et al.*, ref. 32.)

ORNL-DWG 66-10439

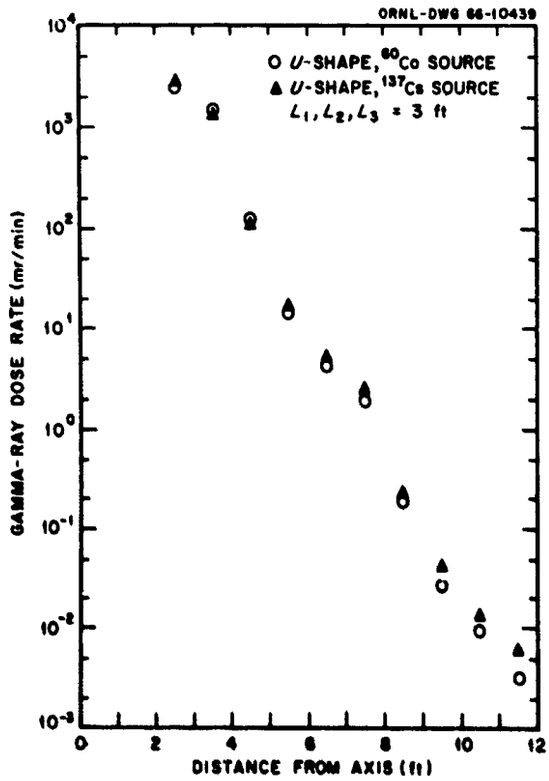

Fig. 5.25. Gamma-Ray Exposure Dose Rates Measured in 1-ft-square U-Shaped Concrete Duct. ^{60}Co and ^{137}Cs Gamma-Ray Sources. (From Terrell *et al.*, ref. 32.)

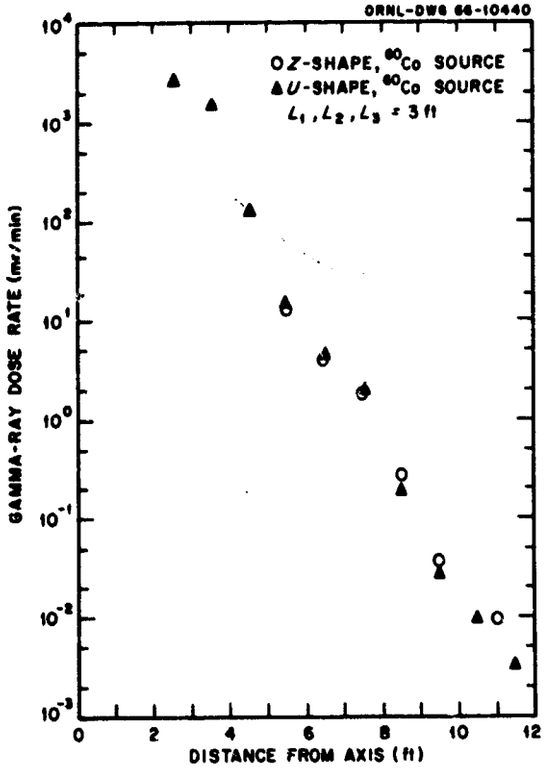

Fig. 5.26. Gamma-Ray Exposure Dose Rates Measured in 1-ft-square U- and Z-Shaped Concrete Ducts: ^{60}Co Source. (From Terrell *et al.*, ref. 32.)

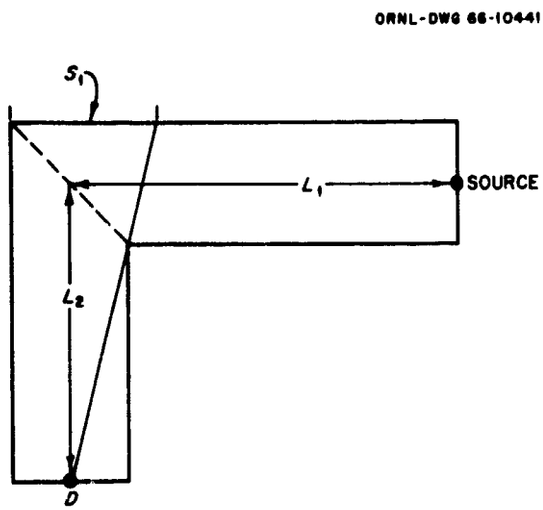

Fig. 5.27a. Schematic of 3-ft-square L-Shaped Concrete Duct (L_1, L_2 = 7.5 ft). S_1 is the area on the long side of L_1 which may be viewed from D. S_1 is 3 × 3.75 ft.

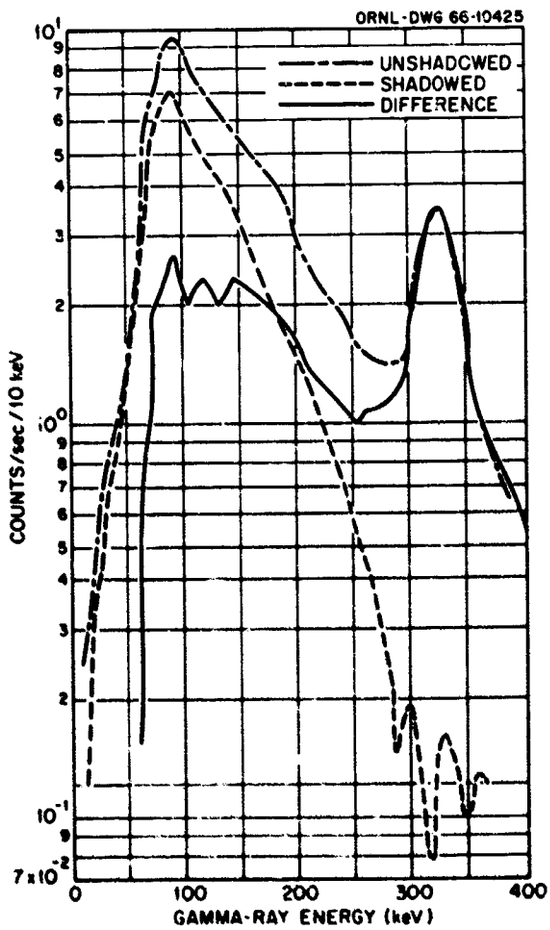

Fig. 5.27b. Gamma-Ray Energy Spectrum at Exit of 3-ft-square L-Shaped Duct With and Without Scattering Area S_1 (see Fig. 5.27a) Shadowed from ^{60}Co Source. (From Chapman, ref. 36.)

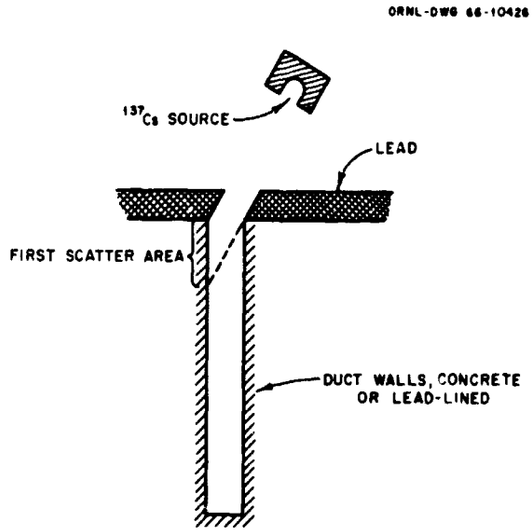

Fig. 5.28*a*. Schematic of Square Concrete Duct Showing First Scatter Area.

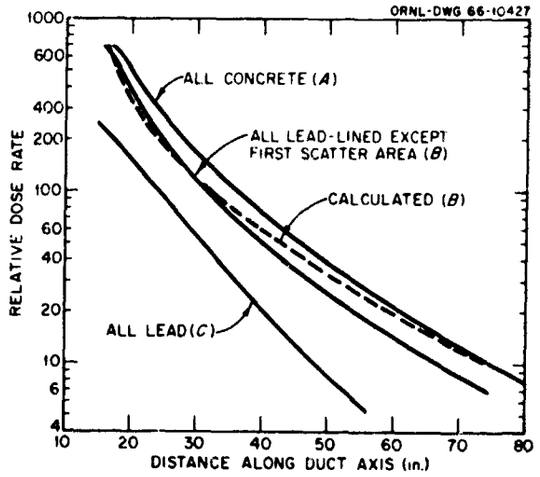

Fig. 5.28*b*. Measurements and Single-Reflection Analysis of Gamma-Ray Dose Rates Along Axis of 8-in.-square Concrete Duct With and Without Lead Linings: ^{137}Cs Source. (From Clifford, ref. 21.)

and also with a lead lining in the entire duct (Condition C). Figure 5.28*b* shows the results of the measurements for all three conditions in the 8-in. duct, together with a single-reflection analysis based on the differential albedo for Condition *B*, and Fig. 5.29 shows the fraction of the total dose which is due to reflection from surfaces not exposed to the primary radiation for all the ducts. It was apparent from the results of all three duct sizes that the multiply reflected component increases to become as much as 20 to 30% of the total dose as the duct length is increased.

Brodeur and Batter[38] used the transmission and backscatter data of Raso[23] to predict the effect of a protruding air vent on the dose rate measured in an underground shelter that was due to a ^{60}Co source above the shelter. The predictions were made to compare with measurements made for the geometry shown in Fig. 5.30*a*. The experimental results are shown in Fig. 5.30*b*, where they are plotted as the dose rate at the detector position *with* the protruding cylinder ($D_{w\ c}$) minus the dose rate *without* the cylinder ($D_{wo\ c}$) divided by the dose rate incident on the cylinder (D_i). The detector was located in several positions below the air vent and various cylinder heights were used. The calculations predicted dose rates that were lower by factors of 2 to 5 than those observed experimentally.

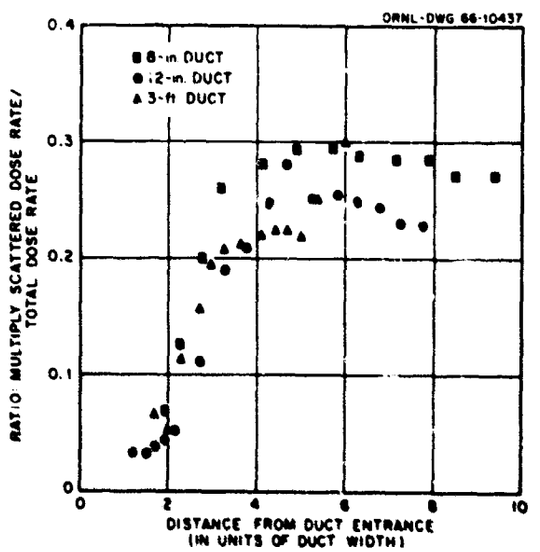

Fig. 5.29. Ratio of Multiply Scattered Gamma-Ray Dose Rate to Total Dose Rate Along Axes of 8-in.-, 12-in.-, and 3-ft-square Concrete Ducts: ^{137}Cs Source. (From Clifford, ref. 21.)

It was pointed out above that Song[13] applied the LeDoux-Chilton albedo technique to the problem of neutron streaming in two legged rectangular concrete ducts, the calculational model being identical in geometric detail with that used

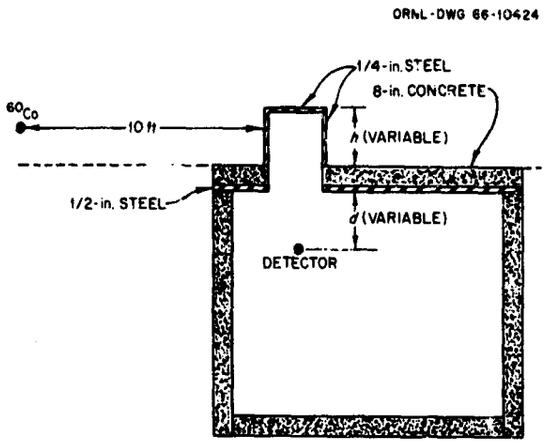

Fig. 5.30a. Schematic of Underground Shelter and Protruding Air Vent.

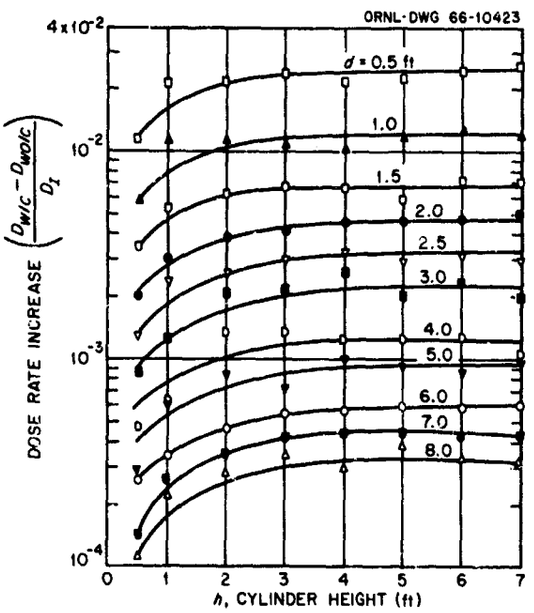

Fig. 5.30b. Measurements of Dose Rates in an Underground Shelter Resulting from Gamma Rays Entering Through a Protruding Air Vent: ^{60}Co Gamma-Ray Source. The solid lines are smooth-curve fits to the data. (From Brodeur and Batter, ref. 38.)

by Chapman[24] for gamma-ray streaming calculations. The duct was assumed to be 3 ft square in cross section, and the sources considered were 14.7- and 2.5-MeV neutrons. The analysis included all single and double scattering events and used a fit to the Monte Carlo data of Allen *et al.*[26] to determine the energy and angular dependence of the neutron dose albedo. A comparison of the results with measurements made by Doty[12] (Fig. 5.31) shows good agreement.* (The solid line represents the calculations for both the 2.5- and the 14.7-MeV sources since there was very little difference between the two sets of results.)

Horton and Halliday[39] used the Simon-Clifford albedo method to calculate the transmission of neutrons through straight cylindrical ducts. The calculations corresponded to an experiment in which 1-, 2-, and 4-in.-diam steel-lined ducts penetrated a water shield that was adjacent to an extended plane source of thermal neutrons. A current albedo, β, of 0.55 was used, and a cosine distribution was assumed. The comparison shown in Fig. 5.32 demonstrates that the Simon-Clifford equation gives good agreement with experiments in which the transmission of thermal neutrons through cylindrical ducts is measured, provided that reasonable assumptions are made for the thermal-neutron albedos.

Cain[17] performed a series of calculations with his original Monte Carlo albedo code that corresponded to experiments in which the ORNL Tower Shielding Reactor II was used as the source and the thermal-neutron fluxes were measured in a three-legged rectangular concrete tunnel connecting two underground bunkers. The bunkers were 12-ft cubes connected by a 3-ft-wide by 8-ft-high tunnel as shown in Fig. 5.33*a*. Two sets of measurements were made, one originating at the center line of the top bunker, in which case the top of the top bunker was left open, and the other originating at the center line of the front bunker, in which case the front of the front bunker was left open. The calculations assumed that the total current albedo for thermal neutrons was 0.8 and that the reflected neutrons had a cosine distribution. The comparison given in Fig. 5.33*b* shows that for this configuration good agreement was obtained between the calculations and the experiment. Cain also used the albedo Monte

*As was discussed in Section 5.1.3, Gardner and Mettler[10] used the ADONIS analog Monte Carlo code to perform calculations corresponding to similar measurements by Doty[12] for a 14.7-MeV source, and they compared these results with albedo calculations made by Song[13] and by Maerker.[14]

Carlo code to calculate thermal-neutron transmission through cylindrical ducts, and obtained results that were in good agreement with those determined by the Simon-Clifford method.

Maerker and Muckenthaler carried out an extensive series of experiments and calculations[30,40] to test the accuracy of the Monte Carlo albedo method as programmed in the AMC code.[27] Three configurations of a 3-ft-square duct were used: a straight duct 45 ft long, a two-legged duct with a right-angle bend located 15 ft down the first leg, the second leg being 30 ft in length, and a three-legged duct with two right-angle bends, the two bends being located 15 ft down the first and second legs and the third leg being 20 ft in length. In the experiments a neutron beam from the Tower Shielding Reactor II entered each duct through an approximately 1-ft^2 area located at the geometric center of the duct mouth. The neutrons were incident at an angle of 45° to one of the duct walls. This angle of incidence was chosen to serve as a rigorous test of the calculation,

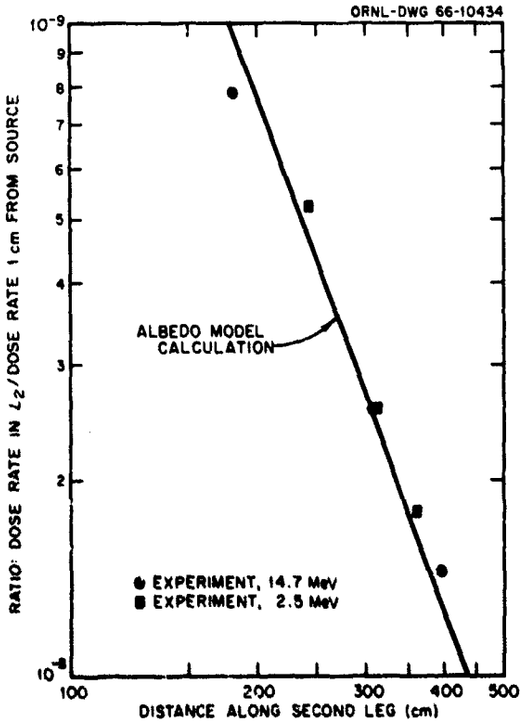

Fig. 5.31. Comparison of Albedo Calculations with Measurements of Neutron Dose Rates in Second Leg of 3-ft-square Two-Legged Concrete Duct: 2.5- and 14.7-MeV Neutron Sources. In the experiment the source was 1 ft outside the duct and L_1 = 15 ft; in the calculation the source was assumed to be at the duct entrance and L_1 = 16 ft. (From Song, ref. 13.)

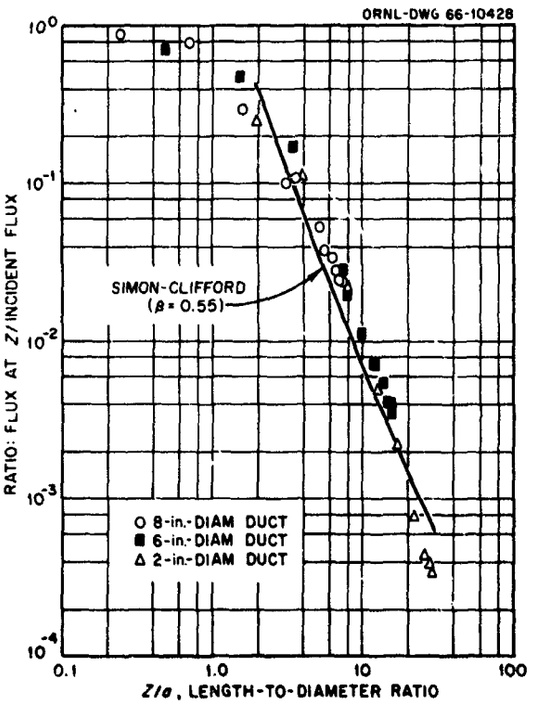

Fig. 5.32. Comparison of Albedo Calculations by Simon-Clifford Technique with Thermal-Neutron Fluxes Measured in Straight Cylindrical Steel-Walled Ducts Through a Water Shield: Plane Source of Thermal Neutrons. (From Horton and Halliday, ref. 39.)

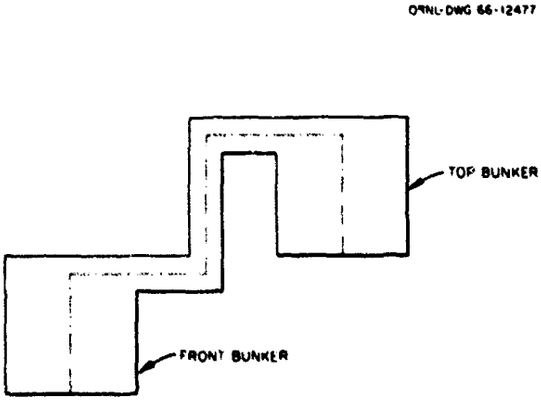

Fig. 5.33a. Schematic of Two Concrete Bunkers (12-ft Cubes) Connected by 3- x 8-ft Tunnel.

since the fluxes and doses for detector locations greater than a few feet from the duct mouth would then be due entirely to wall-scattered radiation. The measured absolute energy spectrum of the beam was used for the source spectrum in the calculations.

Figure 5.34 shows a comparison of the calculated and measured results for fast neutrons. In general, the agreement averages better than 20% through five orders of fast-neutron dose attenuation. In the case of subcadmium or thermal fluxes that result from an incident beam of subcadmium neutrons (Fig. 5.35), the agreement is within 20% in the second and third legs and within 5% for most of the straight ducts.

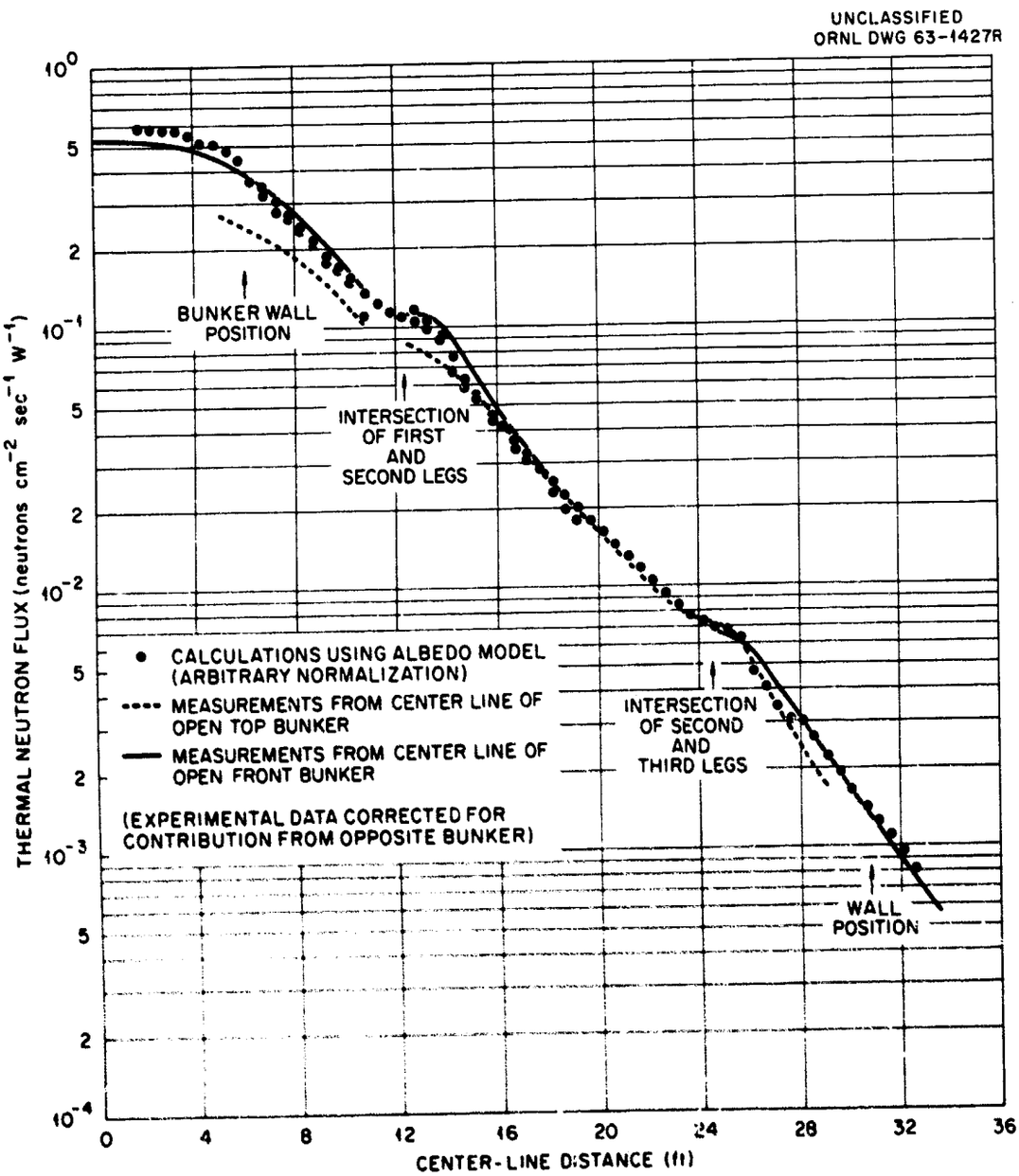

Fig. 5.33b. Comparison of Monte Carlo Albedo Calculations with Measurements of Thermal-Neutron Fluxes in Three-Legged Rectangular Concrete Tunnel. (From Cain, ref. 17.)

In order to test the accuracy of the slowing-down model used in the code, calculations were also made of the thermal-neutron flux resulting from all source neutrons with energies above cadmium cutoff. The comparison between calculations and experiment shown in Fig. 5.36 indicates that the agreement is about the same as that obtained for incident subcadmium neutrons. The statistical errors, number of wall backscatterings, and running times for the same number of source histories were comparable in the two calculations. It should be noted that the calculations were normalized in each case to the measured number of neutrons incident on the wall of the duct from the source beam.

Calculations were also made of the epicadmium or nonthermal spectra at several locations along the center line of the three-legged duct, and these

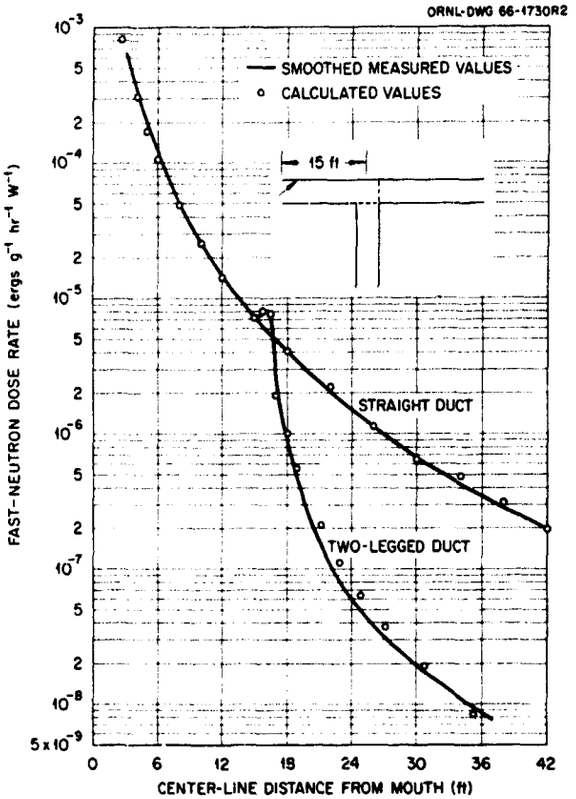

Fig. 5.34. Comparison of AMC Albedo Calculations with Measurements of Fast-Neutron Dose Rates in One- and Two-Legged 3-ft-square Concrete Ducts. The source in the experiment was a collimated beam from the Tower Shielding Reactor II. (From Maerker, ref. 14.)

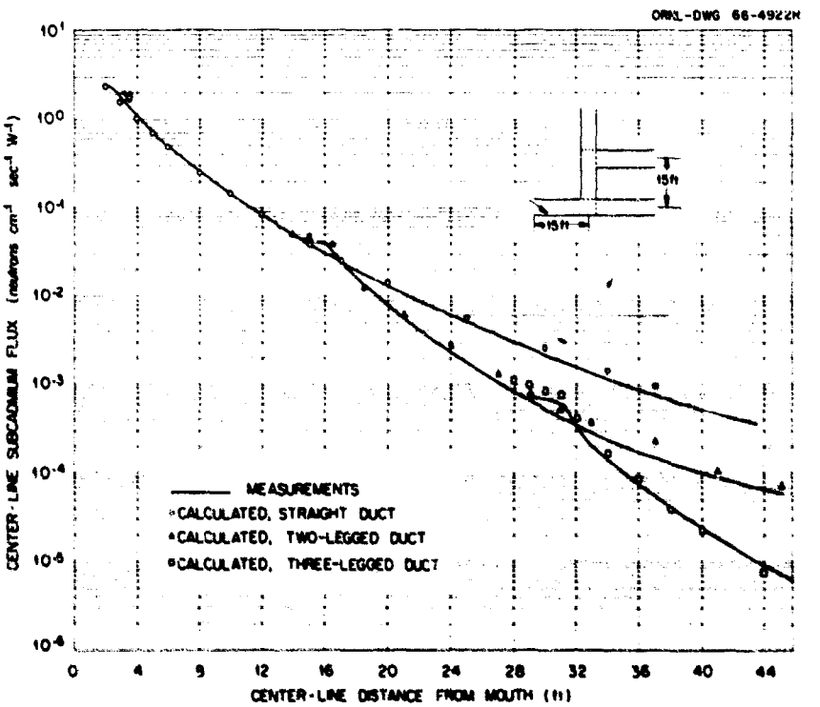

Fig. 5.35. Comparison of AMC Albedo Calculations with Measurements of Thermal-Neutron Fluxes in One-, Two-, and Three-Legged 3-ft-square Concrete Ducts Due to Incident Subcadmium Neutrons. (From Maerker, ref. 14.)

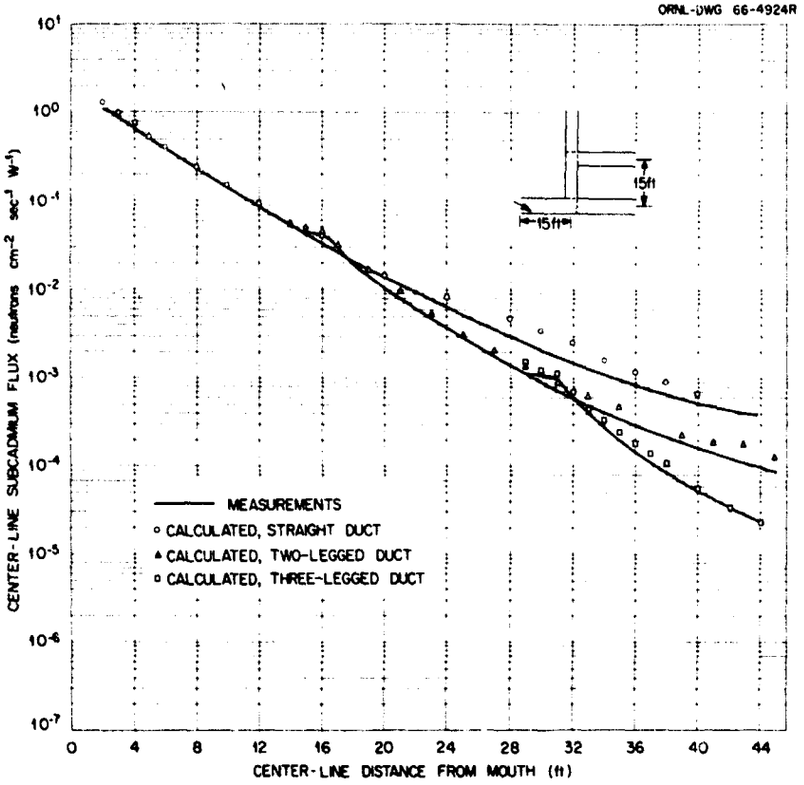

Fig. 5.36. Comparison of AMC Albedo Calculations with Measurements of Thermal-Neutron Fluxes in One-, Two-, and Three-Legged 3-ft-square Concrete Ducts Due to Neutrons Having Energies Above Cadmium Cutoff. (From Maerker, ref. 14.)

Table 5.5. Comparison Between Calculated and Measured Epicadmium Multicollision Dose Rates in Three-Legged Duct

Duct Leg	Distance from Mouth to Detector (ft)	Dose Rate (ergs g^{-1} hr^{-1} W^{-1})		
		Measured*		Calculated
		10-in. Ball	12-in. Ball	
2	19	$2.5 \times 10^{-6}(2.1 \times 10^{-6})$	$1.35 \times 10^{-6}(1.1 \times 10^{-6})$	1.9×10^{-6}
2	23	$5.5 \times 10^{-6}(4.9 \times 10^{-7})$	$2.85 \times 10^{-7}(2.45 \times 10^{-7})$	4.5×10^{-7}
2	29	$1.28 \times 10^{-7}(1.2 \times 10^{-7})$	$6.6 \times 10^{-7}(6.1 \times 10^{-8})$	1.05×10^{-7}
2	33	$1.45 \times 10^{-8}(1.2 \times 10^{-8})$	$6.4 \times 10^{-9}(4.8 \times 10^{-9})$	9.2×10^{-9}
3	40	$1.08 \times 10^{-9}(9.0 \times 10^{-10})$	$6.0 \times 10^{-10}(5.1 \times 10^{-10})$	6.5×10^{-10}

*The dose rates in parentheses are those obtained when the center of detection was assumed to be at the center of the polyethylene ball rather than at its leading edge.

spectra, together with the flux-to-multicollision dose factors of Snyder and Neufeld,[41] were used to calculate the epicadmium multicollision dose rates at the same locations. The results are compared in Table 5.5 with measurements made with a dosimeter designed to give a response proportional to the Snyder-Neufeld multicollision dose curve over the range of interest. The dosimeter was a spherical BF_3 counter placed inside a 10- or 12-in.-diam polyethylene ball covered with cadmium.

5.1.5. EMPIRICAL CORRELATION FOR RECTANGULAR DUCTS

From the background of experimental and analytical data available, Ingold and Huddleston[35] developed an empirical formula for estimating the attenuation of gamma rays in rectangular ducts. By best fit to the data, the formula was found to be

$$\frac{D}{D_0} = 0.214 \frac{(H/W)^{0.907}\, W^{2.864}}{L_1^{2.534}\, L_2^{2.667}\, E_0^{0.710}}, \quad (5.51)$$

where

D = dose rate on axis of duct at point of interest,

D_0 = dose rate 1 ft from the source,

H = height of duct (ft),

W = width of duct (ft),

L_1 = length of first leg measured from the source to the center of the first corner (ft),

L_2 = length of second leg measured from the center of the corner to the detector (ft),

E_0 = gamma-ray source energy (MeV).

Use of this formula is limited to problems which meet the following criteria:

Point source at duct entrance, $0.662 \text{ MeV} \leqq E_0 \leqq 6.0 \text{ MeV}$

$1.0 \leqq H \leqq 6.0$ ft

$1.0 \leqq W \leqq 6.0$ ft

$2 \leqq L_1 \leqq 36$ ft

$1 \leqq H/W \leqq 2$

$L_1/H \leqq 6$

$L_2/H \leqq 6$

$L_1/W \geqq 2$

$L_2/W \geqq 2$

While this formula is useful for the case of a point source, it should be applied with caution to the case of a broad-beam source.

Results obtained with Eq. 5.51 are shown in Figs. 5.21 and 5.22 (Section 5.1.4.).

5.2. Methods for Calculating Radiation Transmission Through Shields Containing Voids

5.2.1. RAY ANALYSIS TECHNIQUE FOR SINGLE VOIDS

There will be situations in which a shield will contain irregularities that are not classifiable as ducts but which, like ducts, cause the flux at nearby points on the shield surface to be increased simply because the amount of attenuation offered by that region of the shield has been reduced. Such irregularities, which can vary in size and shape, are usually referred to as "voids." In general, voids do not extend either to the source or to the shield surface, but methods applied to them can also be used to treat depressions in shield surfaces.

The technique most frequently applied to single voids is the ray analysis technique, which is described in Section 5.1.2 in connection with duct

transmission problems. As is pointed out there, the basic assumption of the ray analysis technique is that the radiation transmission is a function only of the path lengths through each material or void encountered along a straight line between the source point and the point of interest. When applied to voids, the increase in the flux on the shield surface is determined by the difference in the fluxes calculated with and without the void present.

Consider, for example, the case of a disk-shaped void in a semi-infinite slab shield adjacent to an infinite plane gamma-ray source with the ends of the disk parallel to the infinite dimension as is shown in Fig. 5.37. Let $\Phi(L)$ be the flux of energy E at a point on the surface of the shield with no void, and $\Phi(L - t)$ be the flux with the void present. For the latter the point of interest is the intersection of the center line of the void with the shield surface. The influence of the void is estimated by performing a point kernel integration over the source plane to obtain $\Phi(L)$ and $\Phi(L - t)$.

To calculate the flux for the plane shield of thickness L, define $b_1 = \sum_i \mu_i t_i$ over L normally through the shield. The contribution of a ring-shaped source with a particle emission rate of N_0 at an angle θ from the detector would then be

$$d\Phi = \frac{N_0}{2} \frac{dr}{r} e^{-b_1 \sec\theta} . \qquad (5.52)$$

ORNL-DWG 66-10404

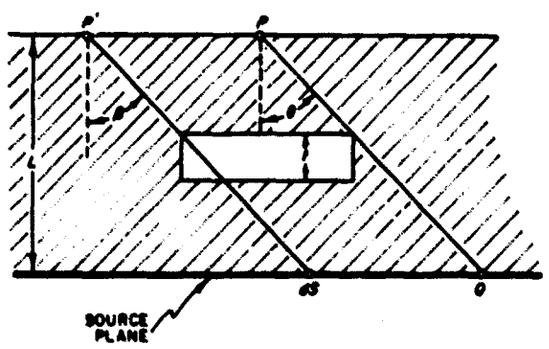

Fig. 5.37. Geometry for Calculating Effect of Disk-Shaped Void on Radiation Transmission Through Shield.

Integrating over the plane source out to an angle θ gives

$$\Phi(\theta) = \frac{N_0}{2} \int_{b_1}^{b_1 \sec\theta} \frac{e^{-t}}{t} dt , \qquad (5.53)$$

where $t = b_1 \sec\theta$. Since by definition

$$E_1(x) = \int_x^\infty \frac{e^{-t}}{t} dt , \qquad (5.54)$$

then

$$\Phi(\theta) = \frac{N_0}{2} [E_1(b_1) - E_1(b_1 \sec\theta)] , \qquad (5.55)$$

and integrating over the entire source plane gives

$$\Phi(L) = \frac{N_0}{2} E_1(b_1) . \qquad (5.56)$$

If the gamma-ray number buildup through b_1 is B_1, then $\Phi(L)$ may be estimated by

$$\Phi(L) = \frac{N_0 B_1}{2} E_1(b_1) . \qquad (5.57)$$

The buildup factor used here as a simple multiplier is only symbolic since the buildup factor is really part of the kernel that is integrated over all space. As is pointed out in Chapter 3, when the Taylor form of the buildup factor is used, the form of these equations is unchanged and the buildup effect is simply included by modifying the arguments of the exponential functions. Actually in these problems it is sufficiently accurate to use the equation as it stands and to determine B_1 only on the basis of the slant penetration (Q to P) that grazes the void. For B_2, an average of B_1 and of the buildup factor based on the minimum path length normal to the void is usually quite adequate. Using the arithmetic mean will always produce a conservative result since this gives equal weight to the buildup factor from a region of lesser importance.

Now to calculate the flux for a shield in which a disk-shaped void intercepts at an angle θ from

the point P, define $b_2 = \Sigma\ \mu_i t_i$ over $(L - t)$. Then for angles less than θ

$$\Phi_1 = \frac{N_0 B_2}{2} [E_1(b_2) - E_1(b_2 \sec \theta)] , \quad (5.58)$$

and for angles greater than θ

$$\Phi_2 = \frac{N_0 B_1}{2} E_1(b_1 \sec \theta) . \quad (5.59)$$

Thus the total flux is

$$\Phi(L - t) = \Phi_1 + \Phi_2 = \frac{N_0 B_1}{2} E_1(b_1 \sec \theta) + \frac{N_0 B_2}{2} [E_1(b_2) - E_1(b_2 \sec \theta)] , \quad (5.60)$$

and the difference, $\Phi(L - t) - \Phi(L)$, is the increase in the flux at point P due to the presence of the void. Because P is centered over the void, it will be the point of maximum flux increase.

For points offset from the center, for example, for point P' in Fig. 5.37, Eq. 5.60 will not be valid. If the source is isotropic, the increase in the contribution at P' by a source surface increment dS caused by the void is given by

$$\Phi_i = \frac{N_0 dS}{2\pi(L \sec \beta)^2} \times [B_3\, e^{-\mu(L-t)\sec\beta} - B_4\, e^{-\mu L \sec\beta}] , \quad (5.61)$$

where B_3 and B_4 are the buildup factors along the path $dS \rightarrow P'$ with and without the void present respectively. If the source is a cosine source, the increase is given by

$$\Phi_c = \frac{N_0 dS \cos\beta}{\pi(L \sec \beta)^2} \times [e^{-\mu L \sec\beta} - e^{-\mu(L-t)\sec\beta}] . \quad (5.62)$$

The integral of Eq. 5.61 or 5.62 over the appropriate source area will give the total increase in flux at P' due to the presence of the void. The appropriate source area includes all points for which a ray to P' passes through the void. In most practical situations this integral must be evaluated numerically. The value of the integral at representative points will serve to determine the shape and thickness of the shield patch required to negate the effect of the void.

A simple approximate form of ray analysis given by Tonks[42] may be applied to certain problems involving voids or depressions in a very thick shield. This method considers first the flux at a point on the surface of a uniform infinite slab shield whose thickness is equal to the ray of minimum length through a void or depression in the shield. It then accounts for the reduction in flux due to the longer material path of nearby rays terminating at the same point. The method is based on the fact that the formula for the flux through an infinite slab,

$$\Phi = \frac{N_0}{2} E_1(\mu t) , \quad (5.63)$$

may be approximated by

$$\Phi \cong \frac{N_0}{2\mu t} e^{-\mu t} \quad (5.64)$$

for $\mu t \gg 1$ with an error that is approximately equal to $1/\mu t$.

The application of Tonks' approximation is as follows. Consider a slab shield with a void such as that shown in Fig. 5.38. Let the ray passing through Q and P be the path of minimum material penetration, t_0, and let it coincide with the z axis. In many cases nearby rays may be expressed as

$$t \cong t_0 + \frac{1}{2} a\theta_x^2 + \frac{1}{2} b\theta_y^2 , \quad (5.65)$$

where θ_x and θ_y are the angles between the minimum ray and a nearby ray projected onto the xz and yz planes respectively and a and b are determined by the specific geometry. Substituting Eq. 5.65 into an approximation analogous to Eq. 5.64 yields for the flux Φ' at P

$$\Phi' = N_0 \frac{e^{-\mu t_0}}{\mu \sqrt{ab}} , \quad (5.66)$$

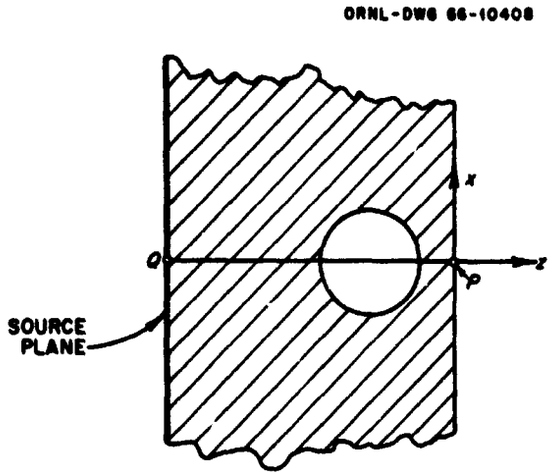

Fig. 5.38. Geometry for Calculating the Effect of a Void in a Shield by Tonks' Approximation.

if both a and b are greater than zero. The ratio of the flux estimated by Eq. 5.66 to that estimated by Eq. 5.64 (for a slab of minimum penetration) is

$$\frac{\Phi'}{\Phi} = \frac{t_0}{\sqrt{ab}}, \tag{5.67}$$

which, provided that $\sqrt{ab} > 1$, gives the increase in effectiveness at P of the shield with a void over that of a simple slab whose thickness is equivalent to the minimum ray.

The limit of θ_x and θ_y for which Tonks' approximation is valid is set by $\theta_x - \theta_y < \alpha$, where α is given by $\alpha = \sqrt{2/\mu t_0}$. As an example, for a spherical void of radius R_v whose center lies at a depth R from the outside surface of a slab shield of thickness T, it can be shown that the length of a ray near the minimum ray is given by

$$t = t_0 + \left(\frac{T}{2} + \frac{R^2}{R_v}\right)\theta_x^2 + \frac{t_0}{2}\theta_y^2, \tag{5.68}$$

and the increased effectiveness at the minimum-ray terminus is given by

$$\frac{\Phi'}{\Phi} = \frac{t_0}{\left[\left(\frac{T}{2} + \frac{R^2}{R_v}\right)\frac{t_0}{2}\right]^{1/2}}. \tag{5.69}$$

Other expansions of $t = t_0 + f(\theta_x,\theta_y)$ may be derived which would lead to equations of the approximate form of Eq. 5.66.

5.2.2. FLUX PERTURBATION TECHNIQUE FOR SINGLE VOIDS

Kouts[43] treated the problem of voids on the basis of one-velocity transport theory. Instead of using the boundary conditions of the differential transport equation to describe the void, he accounted for it by the way in which the kernel of the integral equation is defined. The effect of the void is then calculated as a perturbation of the flux in a homogeneous medium (no-void case). The method is applicable to either gamma rays or neutrons.

Using this approximation to the transport equation, Kouts investigated the effect of spherical voids in water and obtained good agreement with experiment when he chose certain constants in the solution by fitting to the experimental data at one point. The expression derived for a spherical void in the geometry shown in Fig. 5.39 has the form

$$\Phi(P) = \frac{BV}{2}\int_0^1 d\mu\, \mu^k \exp\left(\frac{2R\mu^2}{L}\right), \tag{5.70}$$

where

$\Phi(P)$ = flux at point P,

B = constant in the approximation to the angular distribution of the scattered flux used by Kouts, that is,

$$\int d\Omega\, \Phi(\Omega)\Sigma p(\Omega' \to \Omega) = B\cos\theta,\ 0 < \theta \leq \frac{\pi}{2}$$

$$= 0,\ \frac{\pi}{2} < \theta < \pi,$$

Σ = total macroscopic cross section,

$p(\Omega' \to \Omega)$ = probability of scattering from direction Ω' to direction Ω,

V = parameter in the expression for flux distribution through the shield in the absence of voids given by $\Phi_0 = V\Phi(\Omega)\, e^{-3/b}$,

R = radius of void,

L = shield thickness,

b = number of relaxation lengths in the shield material,

$\mu = \cos \theta$.

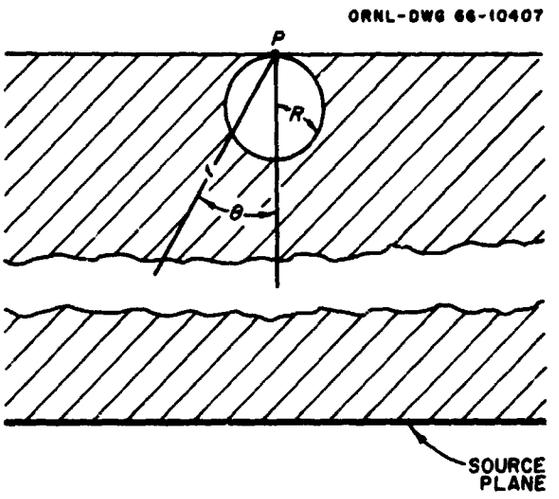

Fig. 5.39. Geometry for Calculating Effect of Void in Shield by Kouts' Technique.

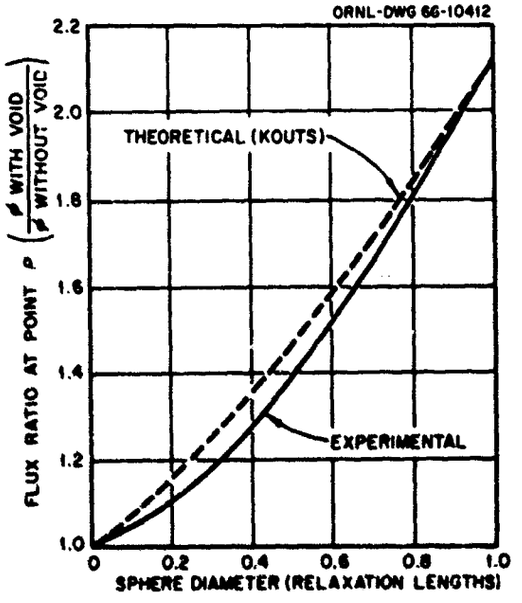

Fig. 5.40. Comparison of Flux Increase Due to Spherical Void in Water Shield Calculated by Kouts' Technique with That Determined by Experiment. (From Kouts, ref. 43.)

A best value of $k = 4.5$ was chosen by Kouts by fitting experimental data for gamma rays at $2R/L = 1$.

Results obtained with this equation are compared in Fig. 5.40 with experimental data for gamma rays.

5.2.3. TECHNIQUE FOR SMALL RANDOMLY SPACED VOIDS

For the case of a large shield containing small randomly spaced voids which are small in distance across relative to the relaxation length of the radiation (for example, a gamma-ray shield consisting entirely of iron shot), the effect of the voids on the radiation transmission is obtained simply by increasing the relaxation length used in the calculation of the shield attenuation by the ratio of the average density of the shield to the density of the solid material used in the shield.

When the voids are not negligibly small, however, it can be shown that on a statistical basis the penetrating radiation will be greater than would be predicted by using an average density. Consider, for example, two normal rays through the shield, one which is the average penetration t plus an increment δ and one which is shorter than average by the same increment. Their average penetration is

$$\frac{1}{2}\left[e^{-\mu(t+\delta)} + e^{-\mu(t-\delta)}\right] = e^{-\mu t}\cosh \delta\mu > e^{-\mu t}.$$

Thus, although their average penetration distance is t, their average penetration is greater than $e^{-\mu t}$.

This problem has been treated statistically by Smith,[44] who arrived at an effective thickness t_e given by

$$t_e = \frac{t(1-v)}{1 + 0.55sv^2}, \qquad (5.71)$$

where t is the actual thickness, v is the fraction of the volume which is void, and s is the average distance between voids measured in relaxation lengths. An equivalent expression for an effective

attenuation coefficient is

$$\mu_e = \frac{\mu(1-v)}{1 + 0.55\,(s/\mu)\,v^2} \qquad (5.72)$$

or, generalized to the case where the voids contain a material of attenuation coefficient μ', is

$$\mu_e = \frac{\mu' + (1-v)(\mu-\mu')}{1 + 0.55\,(s/\mu)\,(\mu-\mu')\,v^2} . \qquad (5.73)$$

Appendix 5A. Machine Programs

Several machine programs that utilize either the ray analysis or the analog Monte Carlo technique described in Sections 5.1.2 and 5.1.3 respectively are broadly outlined below to aid the reader in deciding which of these particular programs most nearly applies to his particular situation. It is emphasized that other good computer codes are available and new ones are constantly being developed. Further information on shielding programs, including the availability of the program decks, libraries, and utilization instructions, may be obtained from the USAEC Radiation Shielding Information Center at Oak Ridge National Laboratory, P. O. Box X, Oak Ridge, Tennessee.

5A.1. RAY ANALYSIS PROGRAMS

Some common features of computer programs utilizing the ray analysis or point-kernel techniques are as follows:

(1) The source-shield geometry is described as a series of simple geometric regions.

(2) The source is divided into a number of regions, and the radiation emitted from each region is assumed to come from a point concentrated at its center.

(3) The flux or some response to flux (exposure dose, heating, etc.) is calculated at designated points by summing the contribution from each of the source points.

C-17 and L-63 Codes. – The General Dynamics C-17 and L-63 shield penetration programs[45] are identical except for the geometry subprogram. Acceptable geometries for the C-17 program are limited to frusta of rectangular pyramids and coaxial cylinders and their annuli. The L-63 program is more inclusive in that it accepts cylinders, and their annuli, that are defined about arbitrary axes, sectors of these cylinders, and frusta of pyramids whose bases are quadrilaterals, spheres, hollow spheres, hemispheres and spherical sectors. The L-63 program also accepts regions within regions and regions within regions within regions in which the geometry types can be varied.

The geometry routine determines the intercepted distance in each material along each source-detector ray by an iterative stepping point. These distances are used in the gamma-ray and/or neutron routines for calculation of the attenuation along each ray.

The gamma-ray routine calculates the differential gamma-ray energy spectrum at a point detector for each point source. The uncollided flux calculation is carried out in a straightforward manner. The scattered flux is evaluated by means of the NDA moments method data,[46] which give the spectra of scattered gamma rays due to monoenergetic point isotropic sources in an infinite medium as a function of penetration depth. In applying these data to finite media, the influence of material interfaces must be discounted. The total spectrum calculated at a detector point is the sum of the spectra from the individual source points. The total spectrum may then be multiplied

point-wise by either flux-to-exposure-dose or flux-to-heat conversion factors. For materials which are mixtures of elements, an effective atomic weight is determined and the differential number spectra are found by curve fitting to the data of ref. 46. A formula for calculating effective atomic numbers is given in the utilization manual.[45]

Basic data on neutron penetration are not nearly so comprehensive as the data on gamma-ray attenuation. In order to determine the neutron spectrum from an individual point source, a reference material must be selected for which basic penetration calculations have been perfcrmed. All materials along the ray are then assumed to be the reference material. The penetration distances for each material are weighted in accordance with the ratio of the material removal cross section.

QAD Program. – The Los Alamos Scientific Laboratory program QAD[47] accepts any geometry which can be described by a set of cartesian quadratic equations. It cannot calculate differential gamma-ray spectra. A single material buildup factor is used in calculating the dose at a point due to scattered gamma rays. Neutron attenuation is determined by interpolation of basic penetration information for a single base material in a manner similar to the General Dynamics C-17 program (see above).

GE 04-4 Program. – The General Electric Program 04-4[48] may be used to calculate neutron and gamma-ray dose rates around complex reactor-shield assemblies. It will not compute energy spectra for either type of radiation. Acceptable geometries are those which may be described by rotating rectangles or trapezoids about an axis or by translating rectangles.

Scattered gamma-ray dose is determined by a fit to buildup factors taken from the NDA moments method data.[46] The buildup as a function of penetration is approximated[49] by a series of polynomial coefficients for each material and energy group. Buildup factors for laminated shields are computed using the formulas derived for lead-water and iron-water combinations by Kalos.[50] The assumption is made that these expressions may be applied to other material combinations.

Fast-neutron attenuation is calculated using an approach suggested by Albert and Welton.[51] In this theory collisions with hydrogen are treated as absorptions, and an approximate relation is used to describe the total cross section as a function of energy. For the calculation of attenuation by materials other than hydrogen, exponential attenuation is assumed and the cross sections are treated as energy-independent adjustable parameters to be determined by best fit to experimental data. This treatment is based on the assumption that heavy materials along the ray are followed by sufficient hydrogen to make removal theory valid.

5A.2. ANALOG MONTE CARLO PROGRAMS

LO5 Code. – The LO5 Monte Carlo computer routine[52] may be used for analysis of radiation streaming down cylindrical ducts. The atomic density and cross sections of the elements in the material around the duct are used as input, and the duct is defined as a region of zero or reduced density, as appropriate.

The restriction on geometry is that all surfaces must be cylindrical and coaxial between any two planes. Since geometry-dividing planes need not be parallel and the axis may vary freely between consecutive planes, multibend ducts of considerable complexity may be defined. Material composition may vary radially or axially with regions of constant composition being separated by cylindrical surfaces or planes.

Some of the more sophisticated features of the LO5 procedure include: biased sampling from source angular distributions, variance reduction by splitting and Russian roulette at boundaries, and the ability to calculate flux or dose rates at nondirectional point detectors by means of statistical estimation.

Allowable neutron interactions include any combination of isotropic or anisotropic elastic and inelastic scattering in the laboratory or the center-of-mass system. All significant photon interactions are allowed.

ADONIS Code. – The ADONIS Monte Carlo program[11] may be used to analyze neutron or gamma-ray transport in regions which may be expressed as rectangular parallelepipeds. Either straight- or bent-duct streaming may be calculated with this code. The total shield and duct geometry may be described by using up to 80 rectangular parallelepipedal regions. Only right-angle bends are allowed, although bends at other angles may be simulated by a series of short rectangular regions provided that the 80-region limit is not exceeded.

Like the LO5 code, this program also employs splitting and Russian roulette. Flux is calculated on the basis of track length per unit volume in specified regions. Flux may be multiplied by any response function in a region to obtain dose, heating rate, interaction rate, or secondary source strength.

A later version of the ADONIS code, called UNC-SAM, has been used by United Nuclear to determine neutron streaming in a passageway due to a reactor source. Results obtained with this version are reported to be in excellent agreement with experiments.[53]

COHORT Code. – The COHORT Monte Carlo code[54] was written for the analysis of neutrons and gamma rays in complex geometries. Primary advantages of the method are the ability to calculate flux in volume or point detectors and the fact that secondary sources may be analyzed without resort to external hand calculation. The program accepts any geometry which may be described by bounding spherical, hyperbolic, conical, cylindrical, or plane surfaces. All surfaces except planes must be symmetric about a line parallel to the Z axis. COHORT is composed of a family of six codes: SO1 for generating source particles, SO2 for generating secondary source particles, HO1 for generating collision histories, AO1 for analyzing histories to determine flux at a point, AO2 for analyzing histories to determine track length per unit volume, and CO1, an auxiliary program, which is used to interpret and print out binary tapes generated by other programs. All codes are written in FORTRAN IV. Exponential transformation and splitting options are available for variance reduction in the HO1 routine.

O5R Code. – The Oak Ridge National Laboratory O5R Monte Carlo code[55] is a versatile program for the analysis of neutron transport. It provides a particularly detailed treatment of cross sections. Geometry description is limited only by the requirement that surface boundaries be represented by a general quadratic or a plane. Up to 16 media may be represented. Component parts of the program include the following:

XSECT, which consists of a package of nine basic cross-section handling codes. Various components of this package and a separate program called LEGENDRE are used in the preparation and modification of a master cross-section tape and two tapes used by O5R to obtain cross section and angular distribution data.

GEOM, which is the geometry subroutine.

O5R, the "heart" of the program, which is used to generate collision parameters which are stored on a data tape.

The program is incomplete in that the user must provide his own source generation and analysis routines. Additionally, the user must provide a program for processing inelastic scattering events. The user may provide any desired variance reduction in the analysis routine. Splitting and Russian roulette are allowed at boundaries which may be arbitrarily assigned in the geometry routine. Unit sources (all starting parameters the same) may be analyzed without use of a separate source routine.

References

[1]D. M. Chase, "Ducts and Voids in Shields," Chapter 12 in *Reactor Handbook*, Part B., Vol. III, *Shielding*, edited by E. P. Blizard and L. S. Abbott, Interscience Publishers, New York, 1962.

[2]"Effect of Irregularities in Shields," Chapter 8 in *Reactor Shielding Design Manual*, edited by T. Rockwell, McGraw-Hill Book Co., New York, 1956.

[3]B. T. Price, C. C. Horton, and K. T. Spinney, "Effect of Ducts and Voids in Shields," Section 4.12, p. 207, in *Radiation Shielding*, Pergamon Press, New York, 1957.

[4]J. H. Hubbell, R. L. Bach, and J. C. Lamkin, "Radiation Field from a Rectangular Source," *J Res. Natl. Bur. Std.*, C 64, 121 (1960).

[5]D. K. Trubey, *A Calculation of Radiation Penetration of Cylindrical Duct Walls,* Oak Ridge National Laboratory Report ORNL-CF-63-2-64 (Feb. 28, 1963).

[6]R. E. Benenson and A. N. Fasano, *The Transmission of Fission Neutrons Having Energy Above the $S^{32}(n,p)P^{32}$ Threshold by Straight Cylindrical Ducts in Water,* Wright Air Development Center Report WADC-TR 57-89 (February 1957).

[7]D. C. Piercey and D. E. Bendall, *The Transmission of Fast Neutrons Along Air Filled Ducts in Water,* United Kingdom Atomic Energy Authority, Winfrith, Report AEEW-R69 (1962).

[8]D. G. Collins and L. W. McCleary, *A Systemization and Penetration Study for Straight Cylindrical Ducts,* General Dynamics/Fort Worth Report NARF 63-3T (May 1963).

[9]J. D. Marshall, *Analysis of Radiation Streaming Through Single-Bend Ducts,* Air Force Weapons Laboratory Report WL-TR 64-136 (January 1965).

[10]L. B. Gardner and A. J. Mettler, *Monte Carlo Calculations of Neutron Streaming Through Two-Legged-Duct Entranceways,* Naval Civil Engineering Laboratory Report NCEL-TR-379 (June 1965).

[11]B. Eisenman and E. Hennesay, *ADONIS – An IBM-7090 Monte Carlo Shielding Code Which Solves for the Transport of Neutrons or Gamma Rays in Three-Dimensional Rectangular Geometry,* United Nuclear Corporation Report UNUCOR-635 (March 1963).

[12]D. R. Doty, *Dose Measurements for Neutron Streaming in Ducts,* Naval Civil Engineering Laboratory Report NCEL-TR-282 (March 1964).

[13]V. T. Song, *Fast Neutron Streaming Through Two-Legged Concrete Ducts,* Naval Civil Engineering Laboratory Report NCEL-TR-354 (February 1965).

[14]R. E. Maerker, Oak Ridge National Laboratory, unpublished calculations.

[15]A. Simon and C. E. Clifford, "The Attenuation of Neutrons by Air Ducts in Shields," *Nucl. Sci. Eng.* 1, 156–166 (1956).

[16]J. C. LeDoux and A. B. Chilton, *Attenuation of Gamma Radiation Through Two-Legged Rectangular Ducts and Shelter Entranceways – An Analytical Approach,* Naval Civil Engineering Laboratory Report NCEL-TM-383 (January 1961).

[17]V. R. Cain, *Calculations of Thermal-Neutron Flux Distributions in Concrete-Walled Ducts Using an Albedo Model with Monte Carlo Techniques,* Oak Ridge National Laboratory Report ORNL-3507 (January 1964).

[18]R. L. French, *A Last-Collision Approach to Calculating the Angular Distribution of Fast Neutrons Penetrating a Shield,* Radiation Research Associates Report RRA-M41 (June 1964).

[19]C. C. Horton, "The Shielding of Helical Ducts," *Nucl. Sci. Eng.* 6, 525–529 (1959).

[20]M. J. Berger and D. J. Raso, *Backscattering of Gamma Rays,* National Bureau of Standards Report NBS-5082 (July 1958).

[21]C. E. Clifford, *Gamma Shielding Provided by Ducts,* Defense Research Chemical Laboratories Report DRCL-370 (May 1962).

[22]W. C. Ingold, *Some Applications of a Semi-empirical Formula for Differential Dose Albedo for Gamma Rays on Concrete,* Naval Civil Engineering Laboratory Report NCEL-TN-469 (November 1962).

[23]J. D. Raso, "Monte Carlo Calculations on the Reflection and Transmission of Scattered Gamma Rays," *Nucl. Sci. Eng.* 17, 411–418 (1963).

[24]J. M. Chapman, *Computer Calculations of Dose Rates in Two-Legged Ducts Using the Albedo Concept,* Naval Civil Engineering Laboratory Report NCEL-TR-264 (Oct. 24, 1963).

[25]A. B. Chilton and C. M. Huddleston, "A Semi-empirical Formula for Differential Dose Albedo for Gamma Rays on Concrete," *Nucl. Sci. Eng.* 17, 419–424 (1963).

[26]F. J. Allen, A. Futterer, and W. Wright, *Neutron Reflection and Flux Versus Depth for Concrete,* Ballistics Research Laboratories Report BRL-1189 (January 1963).

[27]R. E. Maerker and V. R. Cain, *AMC: A Monte Carlo Code Utilizing the Albedo Approach for Calculating Neutron and Capture Gamma-Ray Distributions in Rectangular Concrete Ducts,* Oak Ridge National Laboratory Report ORNL-3964 (in preparation).

[28]R. E. Maerker and F. J. Muckenthaler, "Calculation and Measurement of the Fast-Neutron Differential Dose Albedo for Concrete, *Nucl. Sci. Eng.* 22, 455–462 (1965).

[29]W. A. Coleman, R. E. Maerker, and F. J. Muckenthaler, "Calculation and Measurement of the Differential Angular Current Albedo for Subcadmium Neutrons Emergent from Concrete Due to Incident Monodirectional Beams of Epicadmium Neutrons," *Trans. Am. Nucl. Soc.* 9, 146 (1966).

[30]R. E. Maerker and F. J. Muckenthaler, "Measurements and Single-Velocity Calculations of Differential Angular Thermal-Neutron Albedos for Concrete," *Nucl. Sci. Eng.* 26, 339 (1966).

[31]C. M. Huddleston and W. L. Wilcoxson, *Gamma-Ray Streaming Through Ducts*, Naval Civil Engineering Laboratory Report-NCEL-TR-289 (February 1964).

[32]C. W. Terrell, A. J. Jerri, and R. O. Lyday, Jr., *Radiation Streaming in Ducts and Shelter Entranceways*, Armour Research Foundation Report ARF 1158-A02-7 (April 1962).

[33]C. W. Terrell, A. J. Jerri, R. O. Lyday, and D. Sperber. *Radiation Streaming in Shelter Entranceways*, Armour Research Foundation Report ARF 1158–12 (October 1960).

[34]C. W. Terrell and A. J. Jerri, *Radiation Streaming in Shelter Entranceways, Final Report*, Armour Research Foundation Report ARF-1158-A01-5 (July 1961).

[35]W. C. Ingold and C. M. Huddleston, *An Empirical Formula for Calculating Gamma-Ray Dose Attenuation in Concrete Ducts*, Naval Civil Engineering Laboratory Report NCEL-TR-349 (November 1964).

[36]J. M. Chapman, *Gamma-Ray Dose Rates and Energy Spectra in a 3-Foot-Square Duct*, Naval Civil Engineering Laboratory Report NCEL-TR-325 (October 1964).

[37]J. M. Chapman and J. S. Grant, *Gamma Ray Attenuation in Coplanar and Noncoplanar Three Legged Ducts*, Naval Civil Engineering Laboratory Report NCEL-TN-658 (November 1964).

[38]R. J. Brodeur and J. F. Batter, *Radiation Reflected into an Underground Shelter by a Projecting Air Vent*, Technical Operations Incorporated Report TO-B 62–10 (March 1962).

[39]C. C. Horton and D. B. Halliday, *The Attenuation of Thermal Neutrons in Cylindrical Ducts Through a Water Shield*, Atomic Energy Research Establishment, Harwell, Report AERE SWP/P-28 (January 1956).

[40]R. E. Maerker and F. J. Muckenthaler, "Calculation of the Fast-Neutron Dose Rate Along the Center Line of Both a Straight and a Two-Legged Square Concrete Duct Using the Albedo Concept and Comparison with Experiment," *Trans. Am. Nucl. Soc.* 9, 147 (1966).

[41]W. S. Snyder and J. Neufeld, *Calculated Depth Dose Curves in Tissue for Broad Beams of Fast Neutrons*, Oak Ridge National Laboratory Report ORNL-1872 (Apr. 13, 1955).

[42]L. Tonks, *Enhancement of Leakage by Internal Voids in a Shield*, Knolls Atomic Power Laboratory Report KAPL-107 (January 1949).

[43]H. J. Kouts, *Theory of Flux Perturbations by Voids in Shields*, Brookhaven National Laboratory Report BNL-1357 (Sept. 15, 1952).

[44]N. M. Smith, Jr., *The Absorption and Scattering of Radiation in Random Aggregates of Pebbles*, Clinton National Laboratory Report CNL-21 (March 1948).

[45]D. M. Peterson, *Shield Penetration Programs C-17 and L-63*, General Dynamics/Fort Worth Report NARF 61-39T (Dec. 29, 1961).

[46]H. Goldstein and J. E. Wilkins, Jr., *Calculations of the Penetrations of Gamma Rays, Final Report*, New York Operations Report NYO-3075 (NDA-15C-41) (June 1954).

[47]R. E. Malenfant, *QAD Notes*, Los Alamos Scientific Laboratory unpublished report (Nov. 10, 1964).

[48]M. A. Capo, W. E. Edwards, J. J. Loechler, and K. A. Paine, *Shielding Computer Program 04-4, Reactor Shield Analysis*, General Electric, ANP Project, Report XDC-59-7-150 (July 1959).

[49]M. A. Capo, *Polynomial Approximation of Gamma Ray Buildup Factors for a Point Isotropic Source*, General Electric, Atomic Products Division, Report APEX-510 (November 1958).

[50]M. H. Kalos, "A Monte Carlo Calculation of the Transport of Gamma Rays," NDA 56-7 (July 31, 1956), and NDA 56-10 (March 1957) (classified), cited by H. Goldstein in *Fundamental Aspects of Reactor Shielding*, p. 225, Addison-Wesley Publishing Co., Reading, Mass., 1959.

[51]R. D. Albert and T. A. Welton, *A Simplified Theory of Neutron Attenuation and Its Application to Reactor Shield Design*, Westinghouse Atomic Power Division Report WAPD-15 (Nov. 30, 1950).

[52]D. G. Collins, *Utilization Instructions for General Application for the L05 Monte Carlo Procedure*, Radiation Research Associates Report RRA-T44 (May 1964).

[53]P. Mittleman, Machine Applications Group, Inc., private communication, 1966.

[54]D. G. Collins and M. B. Wells, *COHORT – A Monte Carlo Program for Calculation of Radiation Heating and Transport*, Radiation Research Associates Report RRA-T62-2 (4 vols) (Sept. 17, 1966).

[55]D. C. Irving, R. M. Freestone, Jr., F. B. K. Kam, R. R. Coveyou, J. G. Sullivan, and H. P. Carter, *05R, A General-Purpose Monte Carlo Neutron Transport Code*, Oak Ridge National Laboratory Report ORNL-3622 (February 1965).